1988

Accelerator waveform synthesis

Jay Wilson Heefner
University of the Pacific

ACCELERATOR WAVEFORM SYNTHESIS

A Thesis Project

Presented to the Graduate Faculty

of the

University of the Pacific

In Partial Fulfillment

of the Requirements for the Degree

Master of Science Electrical Engineering

by

Jay W. Heefner

October 1988

This thesis, written and submitted by

Jay W. Heefner

is approved for recommendation to the Committee on Graduate Studies, University of the Pacific.

Department Chairman or Dean:

Robert A. Neyhouse

Thesis Committee:

D. Dale Dunmire Chairman

Louis L. Regenstein

David F. Beach

Thuan Van Nguyen

Dated 2-27-89

TABLE OF CONTENTS

Page

LIST OF FIGURES iv

Section

1.0 INTRODUCTION 1

2.0 PROJECT DESCRIPTION AND SPECIFICATIONS 5

3.0 DESIGNS CONSIDERED 7

3.1 Shunt and series tube regulators 9

3.2 Summed pulser circuits 12

3.3 Pulse Forming Line (PFL) 14

3.4 Pulse Forming Network (PFN) 18

4.0 PULSE FORMING NETWORKS FOR NON-RECTANGULAR PULSES 20

4.1 Fourier series of continuous waveforms 21

4.2 The simple L-C circuit 21

4.3 Pulser synthesis for a ramp waveform 23

4.4 Pulser synthesis for a trapezoid waveform 26

4.5 Pulser synthesis for rectangular waveforms 30

4.6 Summary of pulser synthesis 31

5.0 COMPUTER SIMULATION 31

5.1 Ramp waveform simulation 32

5.2 Trapezoid waveform simulation 42

5.3 Rectangular pulse simulation 44

Page

6.0 SENSITIVITY ANALYSIS 50

6.1 Sensitivity analysis 50

6.2 Tuning with sensitivity plots 56

7.0 BENCH TEST RESULTS 62

7.1 Eliminating the "bump" 64

7.2 Bench test tuning results 68

7.3 Bench test conclusions and recommendations 73

8.0 PULSE FORMING NETWORKS FOR ILSE 75

9.0 COST AND SCHEDULE 81

10.0 CONCLUSIONS AND RECOMMENDATIONS 82

REFERENCES 86

FIGURES

Figure		Page
1.	Block diagram of ILSE accelerator.[1]	3
2.	Gap voltage waveforms required for ILSE.[1]	4
3.	ILSE magnetic acceleration section. Note: The six, two inch cores will be replaced by three cores each four inches in thickness.	6
4.	Conceptual design of (a) shunt regulator and (b) series regulator.	8
5.	Conceptual design of (a) shunt regulator and (b) series regulator utilizing feedback.	10
6.	Idealized accelerating waveforms for MBE4.[3]	13
7.	(a) Circuit used to produce accelerating waveforms for MBE4 and (b) actual core voltages for various charge voltages.[3]	13
8.	(a,b,c) Current and voltage pulses for a lossless transmission line (d) discharging into a resistive load. The solid and broken lines represent the voltage and current, respectively.[4]	16
9.	Possible characteristic impedance function of a Pulse Forming Line for use on ILSE.[9]	17
10.	Equivalent forms for five-section Guillemin voltage- fed network.[4]	20
11.	(a) Simple L-C circuit. (b) L-R-C circuit.	22
12.	ILSE ramp waveform shown as: (a) a continuous, periodic, even, and (b) a continuous, periodic, odd function of time.	24
13.	Bi-Polar, Guillemin type C network synthesized from fourier series for the odd function of figure 12b.	27
14.	ILSE trapezoid waveform shown as: (a) a continuous, periodic, even, and (b) a continuous, periodic, odd function of time.	28

Page

15. (a) Bi-Polar network synthesized to produce a 1 second, 1 volt ramp pulse. (b) Computer predicted output voltage waveform. 34

16. Computer predicted output voltage waveform for network of figure 15a terminated into a 2.75 ohm load resistance. 36

17. Computer predicted output voltage waveform for network of figure 15a terminated into (a) 5 ohms, and (b) 100 ohms. 36

18. Voltage and energy transfer efficiencies for network of figure 15a versus load resistance. 38

19. (a) Time-scaled bi-polar PFN. (b and c) Computer predicted output voltage waveforms. 40

20. (a) Normalized bi-polar, one ohm, one second PFN used to produce ramp pulses (b) Computer predicted output voltage waveform for odd and even initial capacitor voltages of +/- 1 volt, respectively. 41

21. (a) Bi-polar network synthesized to produce a 1 second trapezoid pulse. (b) Computer predicted output voltage waveform for a 2.75 ohm load resistance. 43

22. Voltage and energy transfer efficiencies versus load resistance for trapezoid network of figure 21a. 45

23. (a) Normalized, bi-polar, one ohm, one second PFN, and (b and c) computer predicted output voltage waveforms for various initial capacitor voltages. 46

24. (a) Computer predicted output voltage waveform for the network of figure 15a. (b) Computer predicted output voltage waveform for network of figure 15a with even numbered (right side of load) sections removed. Initial capacitor voltages are as shown. 48

Page

25. Voltage and energy transfer efficiencies versus load resistance for rectangular network of figure 24a (even sections removed). 49

26. - 37. Simplified sensitivity functions for the components of the normalized bi-polar PFN of figure 23a. 54

38. Computer predicted output voltage for the network of figure 23a when (a) C6 is increased by 20%, and (b) C6 is increased by 20% and C2 is decreased by 20%. 57

39. (a) Computer predicted trapezoid output voltage pulse for the network of figure 23a. (b) Computer predicted output voltage when C6 is increased 20% and C2 is decreased 20%. 58

40. - 44. Actual sensitivities of the output voltage of the network of figure 23a to component variations. Note: The flat portion near t=0 in figures 40 and 41 is a result of the removal of several data points near the beginning of the plot. This was done in order to allow the spreadsheet program to plot the remaining data on a legible scale. 60

45. (a) Theoretical time and impedance scaled network used for bench tests. (b) Computer predicted output waveform for a load resistance of 92 ohms and vcn(0-)= +/- 100 volts for the odd and even sections, respectively. 63

46. Actual network used for bench tests. 65

47. Actual oscilloscope plots of output voltage of the network of figure 46 for (a) vcn(0-)= +/- 50 volts, odd and even sections, respectively, and (b) vcn(0-)= +50 and -16.67, odd and even sections, respectively. 65

48. Actual oscilloscope plots of output voltage of the network of figure 46 for various initial capacitor voltages. 66

49. Computer model of the network of figure 46 with diodes added. 67

Page

50. Computer predicted output voltage waveform for the network of figure 49. 67
51. Computer predicted output voltage of the network of figure 49 with the even harmonic diode voltage superimposed. Note that the diodes are switching at the time the bump occurs. 69
52. Actual oscilloscope plots of the output voltage of the network of figure 46 with the SCR switches replaced by FET's. 70
53. Actual oscilloscope plot of the network output voltage when C6 is increased to (a) 67 pf, and (b) 76 pf. 71
54. Actual oscilloscope plot of network output voltage when vcn(0-)= +25 volts and -8.33 volts, odd and even sections respectively. 72
55. Actual oscilloscope plots of network output voltage showing that the network does indeed approximate a continuous function as opposed to a transient pulse. 74
56. Equivalent circuit for one 4 inch ILSE core. [9] 76
57. Equivalent circuit for three 4 inch ILSE cores connected in parallel. 76
58. (a) Bi-polar, one micro-second, 13.3 ohm PFN. (b) Computer predicted output voltage waveform into the equivalent circuit of figure 57. 78
59. (a) Bi-polar, one micro-second, 11.2 ohm PFN. (b) Computer predicted output voltage waveform into the equivalent circuit of figure 57. 79
60. Normalized, one ohm, one second, bi-polar Pulse Forming Network. 83

1.0 INTRODUCTION

The Induction Linac System Experiment (ILSE) is a heavy-ion fusion (HIF) device that is being designed at Lawrence Berkeley Laboratory (LBL). The machine will be capable of accelerating 16 carbon ion beams, which are subsequently merged into 4 beams, to energies in the neighborhood of 10 MeV (10 million electron- volts). The purpose of the experiment will be to demonstrate the process of simultaneous acceleration and current amplification for a multiple beam accelerator configuration. If this process can be mastered, the beams produced by a machine such as ILSE would be used to implode and heat a deuterium-tritium (D-T) fuel pellet and produce a thermonuclear inertial confinement fusion (ICF) burn. This technology of achieving a fusion reaction using ion beams is referred to as Heavy-Ion Fusion (HIF) [1].

There are two different methods available for accelerating charged particle beams, the induction linear accelerator and the radio frequency linear accelerator with storage rings. The radio frequency linac is used in West Germany and Japan while the induction linac has become the main HIF accelerator candidate in the United States. The induction linac can be thought of as a sequence of single turn transformers in which the primaries are driven by pulse modulators and the charged particle beam forms the single turn secondary. The core material currently being proposed for use on ILSE is an Allied METGLAS. METGLAS is a metal-glass material that comes in long, thin, continuous strips which are wound layer upon layer to produce a core with the desired dimensions. The

insulation between layers of the core material is provided by a silicon coating only several micro- inches thick. METGLAS materials were chosen because they have a high delta-B to increase volt-second capability (the material does not saturate easily), a high electrical resistivity when cut in thin strips to reduce eddy current losses and a moderate to low Hc to ease core reset [2]. A conceptual design of ILSE including expected accelerator parameters is shown in figure 1. The induction portion of the accelerator which is pertinent to this thesis project is labeled "Magnetic Focus Accelerator".

An ion induction linac used for HIF experiments must operate near the space charge limit along most of its length, therefore small errors in the voltages applied to accelerating gaps can produce local unwanted beam bunching and subsequent beam loss. In order to realize the necessary current amplification in an induction linac the accelerating modules must accelerate the tail of the beam more than the head in a preprogrammed fashion. The purpose of these preprogrammed waveforms is to amplify the beam current while keeping the beam current near the transverse space charge limit in order to exploit the high current capability of induction linacs. As can be seen by the desired gap accelerating waveforms shown in figure 2, the acceleration voltages start as triangular function at gap 1 and progressively become shorter in duration and more rectangular as the beam moves further down the linac [1].

Specific Parameters for ILSE

(Based on Straw #3; Jan 12, 1988)

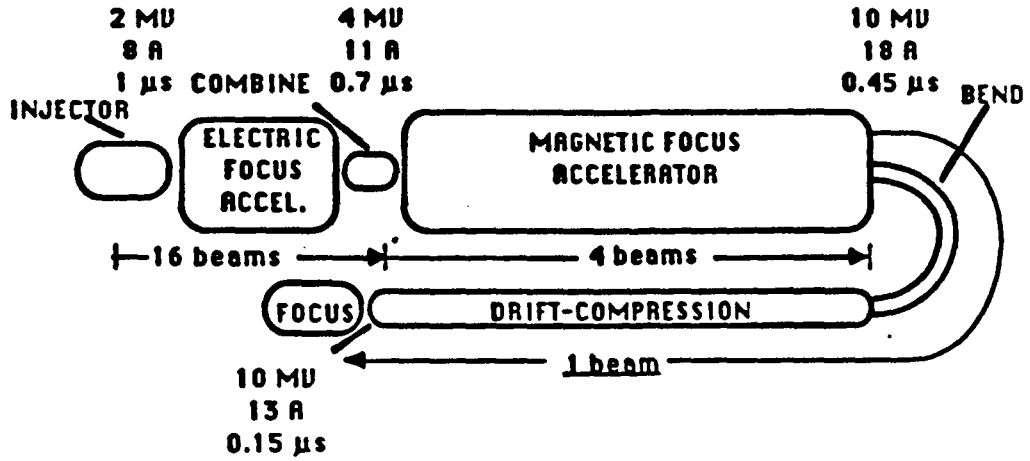

	Injector	Match	E. Acc	Merge	M.Acc1	M.Acc 2	Bend	Drift-C	F.Focus
Ion	C^+	C^+	C^+	C^+	C^+	C^+	C^+	C^+	C^+
Energy(f)	2	2	4	4	6.5	10	10	10	10
Current(f)	8	8	10.8	12.2	16.0	20.5	?	?	?
Pulse(f)	1	1	.74	.66	.5	.39	?	?	?
Tilt(f)	0	0	.24	.24	.15	.098	?	?	0
Period	.4	.4	.4	.5	.5	.6	?	?	0
Length	?	?	9.6	3	7	10.8	?	?	
# Beams	16	16	16	16-4	4	4	1	1	1
Beam size	.016	.018	.018	.029	.026	.023	?	?	?
Sigma 0_h	80	80	70	70-80	80-60	80	80	?	?
Aperture	.027	.027	.027	???	.055	.055	.055	.055	-
Pitch	7	7	7	7-14	14	14	-	-	-
±V-Quad	24.5	24.5	43.8	?					
B-Tip				?	.82	.7/.9	?	?	?
Occupancy	.625	.625	.625	.625	.4	.4	.4	.4	
Emitt.	—	—	—	—	—	—	—	—	

Figure 1- Block diagram of ILSE accelerator.[1]

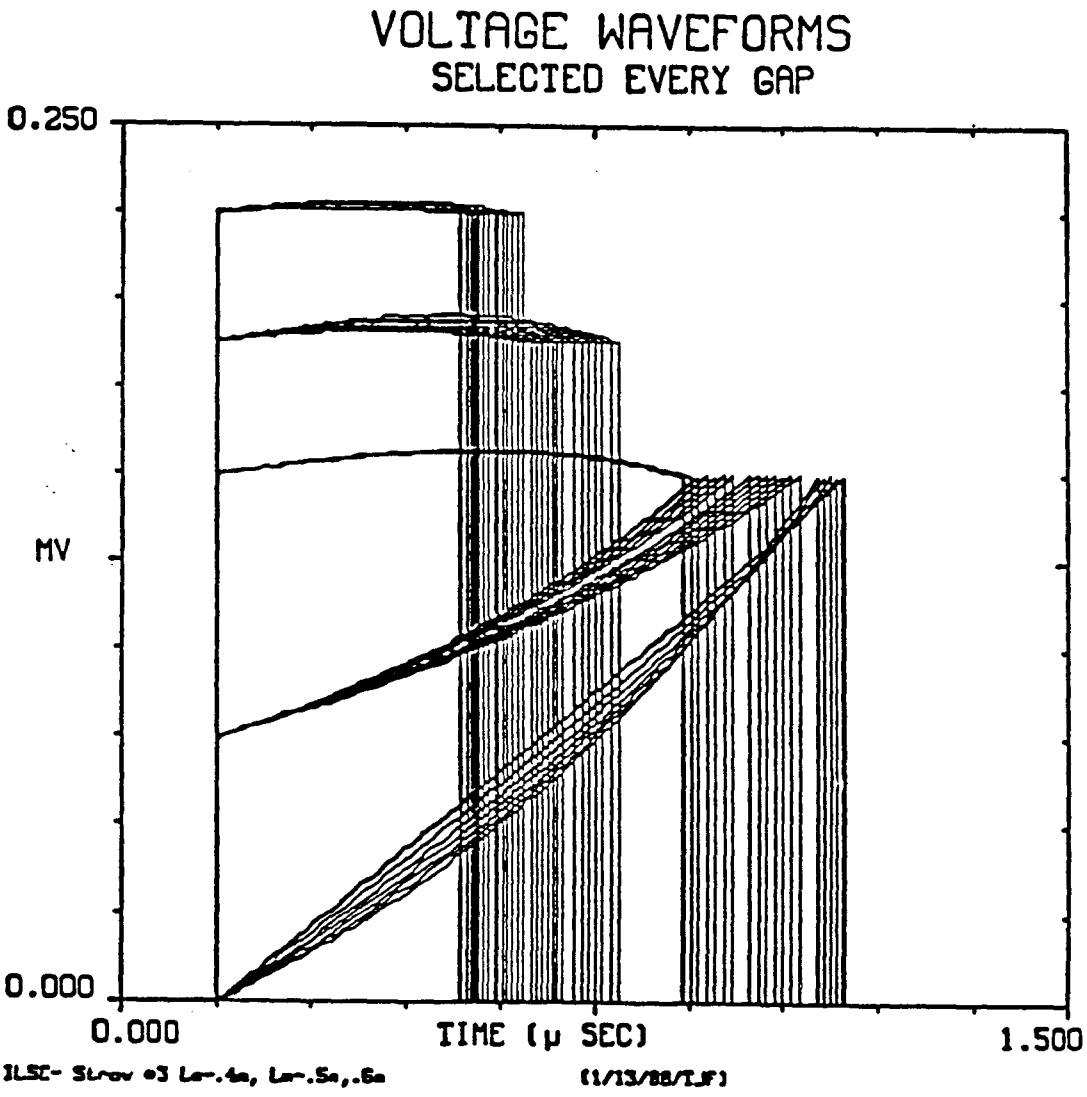

Figure 2- Gap voltage waveforms required for ILSE.[1]

2.0 PROJECT DESCRIPTION AND SPECIFICATIONS

As can be seen by the waveforms plotted in figure 2, the voltages needed to accelerate the ion beams to the desired energies are extremely high (on the order of 200 KV/gap). In addition, because of the load characteristics presented by the core, the currents associated which each waveform are on the order of 2000 amps. Pulsers of this magnitude are not commercially available. The purpose of this project is to design pulsers that will provide the desired waveforms and meet the following specifications:

1. The waveforms shown in figure 2 are simple ramps, trapezoids and rectangles. The pulsers should produce these shapes and have magnitude variations of less than 1 percent. The magnitudes shown in figure 2 are not necessarily the values needed for ILSE, but represent a worst case scenario. The shapes of the waveforms are the important factor. If it is not possible to meet this requirement there is an option to utilize one core of each seven gap section as a "correction core". Early calculations show that rms errors of as much as 10% may be tolerable, but this option should only be used as a last resort.
2. Pulser waveforms should be repeatable to less than 1 percent and any trigger delays repeatable to less than 20 nano-seconds.
3. The pulser used should not preclude the use of other pulsers that will be used in parallel to add "ears" to each end of the waveforms.
4. The core configuration is shown in figure 3. Each gap consists of 3 acceleration cores that can be run individually, in series, or in parallel to produce the necessary waveforms. This is left to the discretion of the designer.

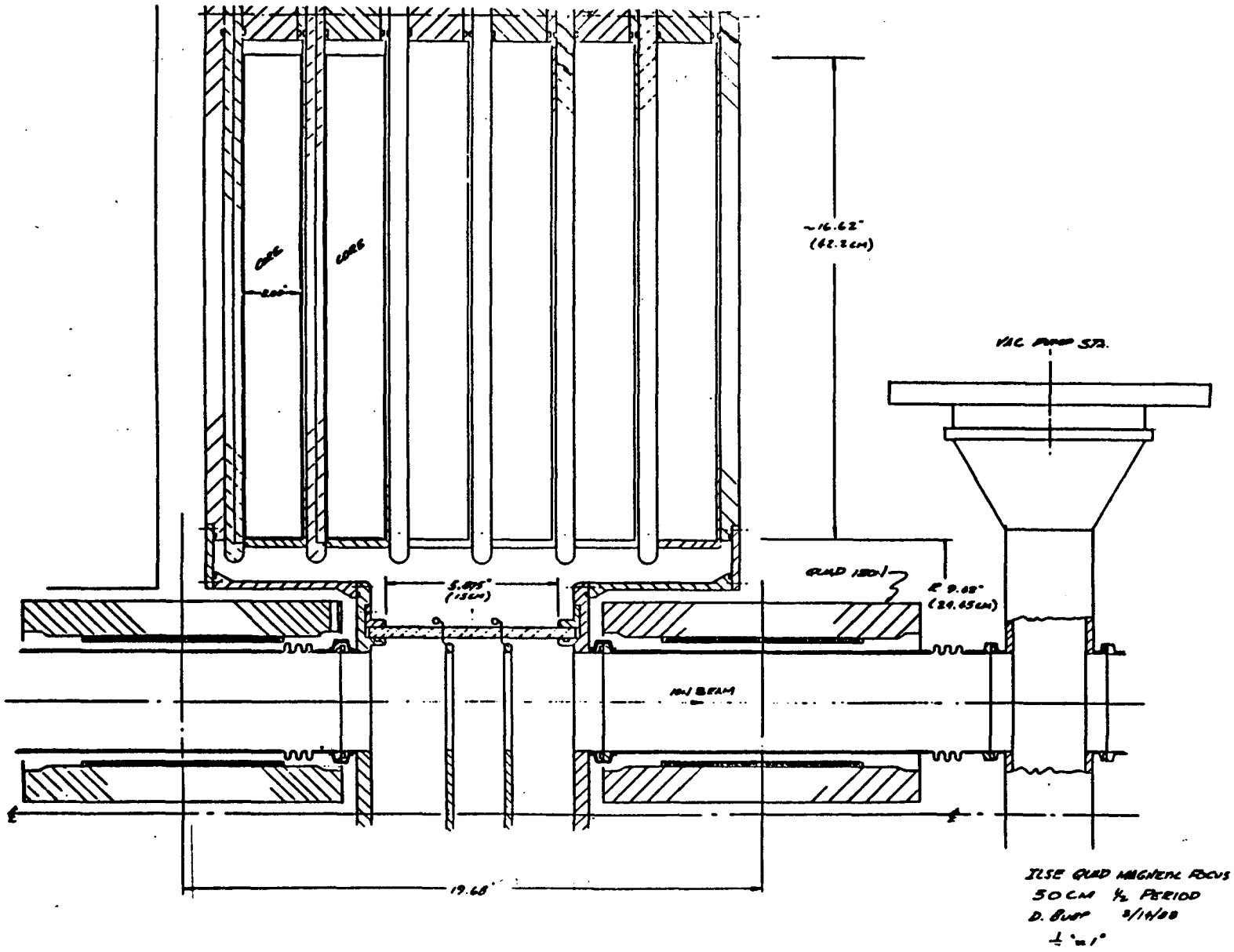

Figure 3- ILSE magnetic acceleration section. Note: The six, two inch cores will be replaced by three cores each four inches in thickness.

The project of designing the pulsers to meet the requirements outlined above is described in this report. The project started with a search for available technologies. Techniques that showed promise were investigated in greater detail and conceptual designs were discussed with ILSE project personnel. Following the conceptual design stage, several of the techniques were used to provide more detailed designs. Each of these designs was then assessed and a decision was made as to which techniques would be tested experimentally. All experimental test set-ups were designed, built, and evaluated by Jay Heefner using equipment available at Lawrence Livermore National Laboratory (LLNL). Experimental results are discussed and designs and recommendations for the ILSE pulsers contained in the appropriate section of this report. An assessment of the feasibility and cost of each pulser is also made.

3.0 DESIGNS CONSIDERED

The specification for the ILSE pulsers did not limit or even suggest the type of pulser designs that were to be considered. Therefore the first step of the project was to brainstorm and research what types of pulser designs had been used in similar designs and possibly adapt one of them to the problem at hand or develop something completely new. Although the choices for pulser designs are virtually limitless, only four types actually showed any reasonable hope for success. They are shunt or series tube regulation, a summed pulser scheme such as that used on a previous HIF machine at LBL, a Pulse Forming Line (PFL), or a Pulse Forming Network (PFN). Each of these ideas is discussed somewhat more in detail in the following paragraphs.

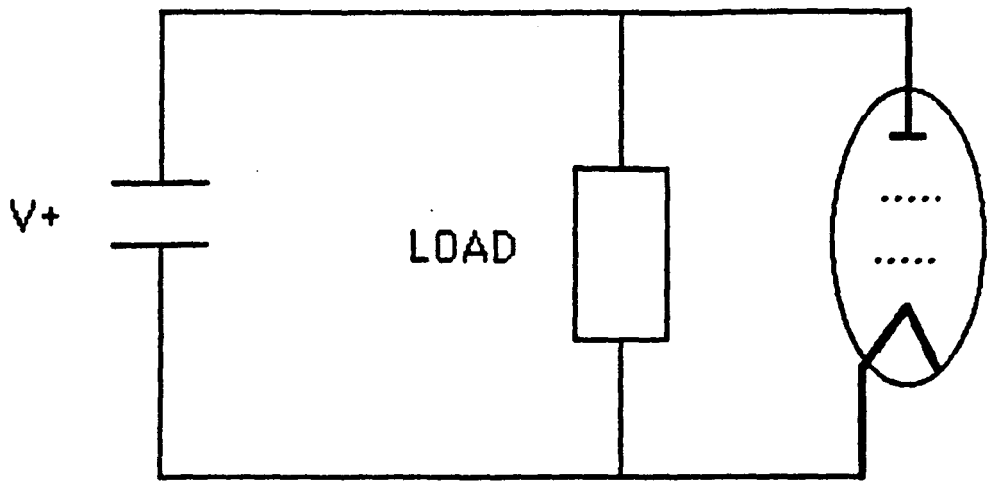

(a)

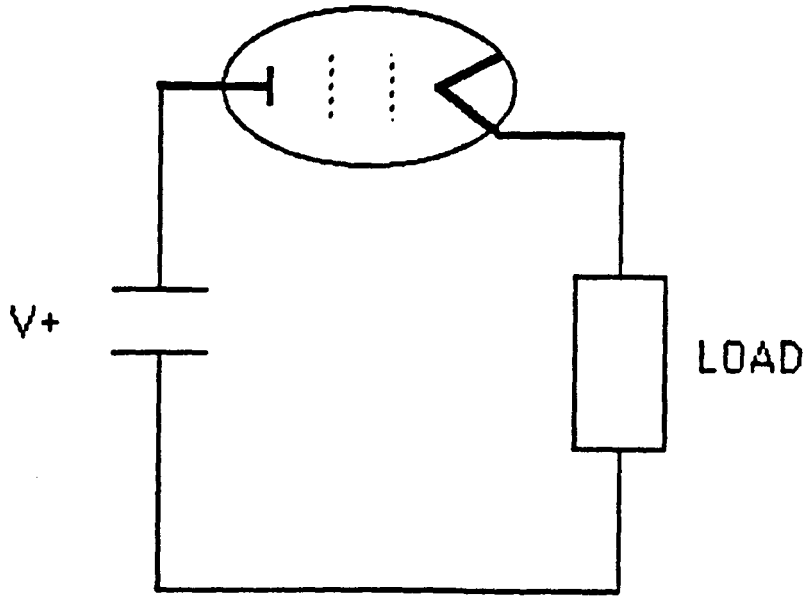

(b)

Figure 4- Conceptual design of (a) shunt regulator and (b) series regulator.

3.1 Shunt and series tube regualtors

Many high voltage pulsed power systems currently in use today employ either a shunt or series tube regulation scheme. Each of these designs is shown schematically in figures 4a and 4b. In the shunt tube regulator configuration of figure 4a the tube is placed in parallel with the load. The current seen by the load is then controlled by adjusting the impedance of the shunt tube. For example, if the amount of current being supplied to the load is too high, the impedance of the tube is adjusted down so that the tube will sink more current. If the amount of current being supplied to the load is too low, then the impedance of the shunt is increased and this in turn increases the load current. As can be seen from this description, the tube is acting as a variable current divider. Just as the shunt tube regulator acts as a variable current divider, the series tube regulator acts as a variable voltage divider. Observe that the series tube regulator of figure 4b is placed in series with the load. In this configuration the impedance of the tube is adjusted such that the load voltage and current are the desired values. For example, if the load voltage or current are higher than desired, the impedance of the tube is increased. This causes the tube voltage to rise and the load voltage to drop, assuming a constant supply voltage. If the load voltage or current are too low, the tube impedance is lowered which in turn causes the load voltage to increase. The description of the series and shunt regulators implies some sort of intelligence on the part of the regulator, i.e. the load voltage or current must be detected and a decision made as to the what value the impedance of the tube must be. This means that some sort of feedback system must be incorporated into the design. Figures 5a and 5b show the shunt

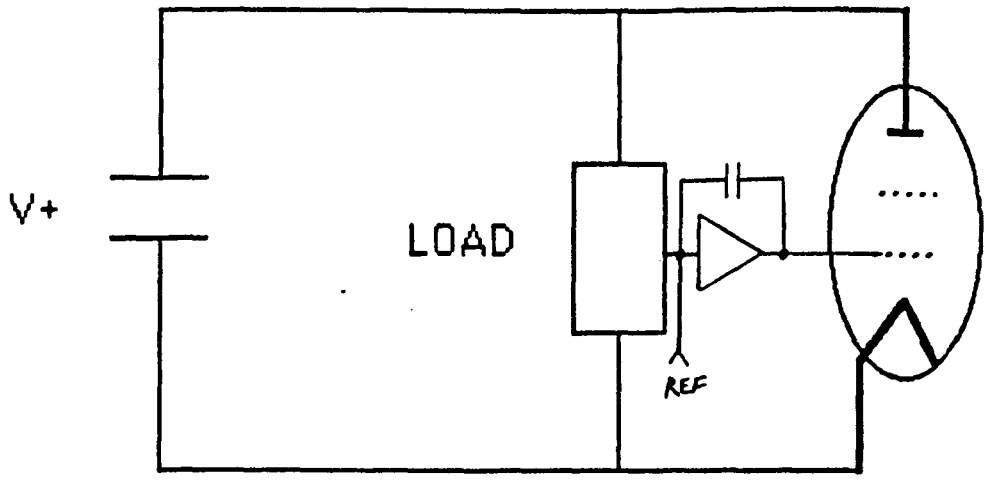

(a)

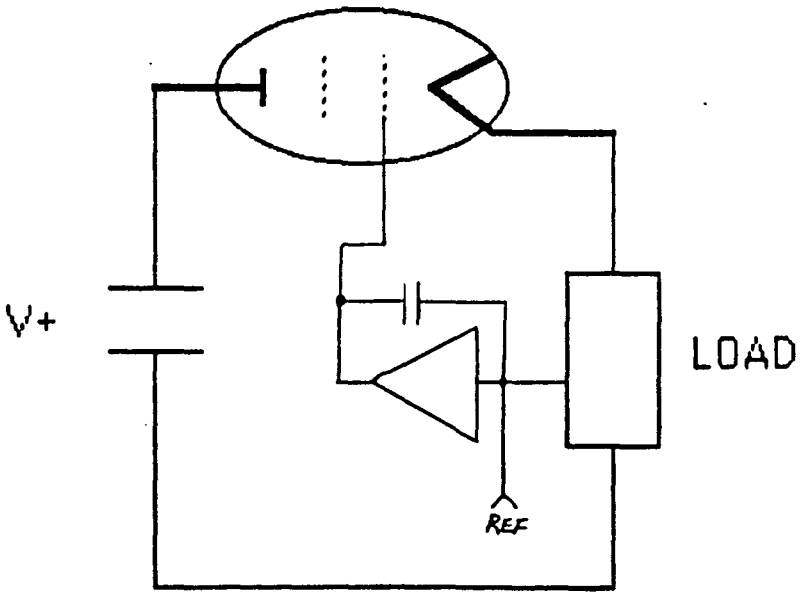

(b)

Figure 5- Conceptual design of (a) shunt regulator and (b) series regulator utilizing feedback.

and series regulator configurations with the feedback system added to the design. The feedback system is one of the major advantages that each of these design configurations possesses. The percent error specification and the repeatability specification are well within the reach of any reasonable feedback system. The shunt and series regulator configurations do not preclude the addition of "ears" to each pulse (specification 3) and in fact if the design of the feedback system is done properly, the ears can be added to the reference pulse that is used by the feedback loop to determine the desired load pulse. The major disadvantage of either of these configurations quickly becomes apparent when the magnitudes of the load voltages and currents are taken into account. If the shunt or series regulator configurations are used, the regulator tube must be able to handle the full gap voltage and maximum supply current. This would mean a tube with a maximum plate voltage in excess of 150 KV and a maximum plate current on the order of 2000 amps. No such tube exists at a cost which is reasonable for consideration. One possible alternative would be to supply the full gap voltage by running each of the 3 cores in the gap (see figure 3) independently. This would lower the plate requirements for the tube to approximately 60 KV and 2000 amps, but the largest tube made by EIMAC has maximum plate ratings of 75 KV and 150 amps (Model Y-676A) and costs on the order of $20,000. Each core pulser would then require 10 of these tubes in parallel which brings the total number of tubes per gap to 30. This means that the minimum cost per gap would then be on the order of $600,000. From past experience and discussions with ILSE project personnel, this cost is completely unacceptable. The only possible way to make a series or shunt regulating scheme competitive would be to build a power supply that produces a rough approximation to the desired

gap waveform and then only use the regulator to "smooth out the bumps". This idea was not pursued because of the fact that if a "rough" power supply could be developed, then it should be possible to develop a power supply that can meet the specifications required in the previous section.

3.2 Summed Pulser Circuits

Lawrence Berkeley Laboratory currently has a multiple beam induction linac in operation. The name of the experiment is MBE4. MBE4 is designed to accelerate four cesium ion beams from approximately 200 KeV to 1 MeV. Twenty-four acceleration gaps are distributed along the 16 meter length of the machine. The ideal waveforms for each of the twenty-four gaps are shown in figure 6. The necessary waveforms are approximated by summing together several different waveforms from separate pulsers. The circuit used to produce these waveforms and the output voltage of the pulser as a function of charging voltage are shown in figure 7. The basic concept employed on MBE4 is that the required gap voltages of figure 2 can be created by triggering, in a predetermined sequence, several pulsers each charged to different voltages. In this manner the desired waveshape can be approximated [3]. Although this method is currently being used successfully on MBE4 there are several major disadvantages to such a system; the first being that, depending on the degree of accuracy desired, many pulser circuits and switches are needed for each accelerating gap. This adds complexity and cost to the system. A second disadvantage is that the waveform produced by a pulser system like this is extremely susceptible to variations in the load characteristics, the charging voltages on the individual sections, and triggering delay and jitter.

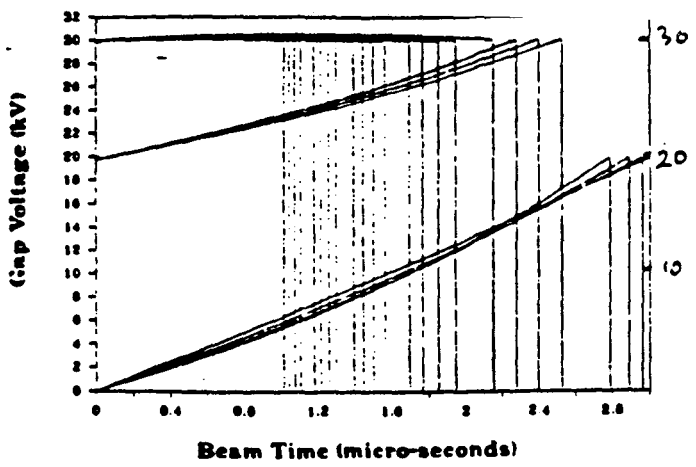

Figure 6- Idealized accelerating waveforms for MBE4.[3]

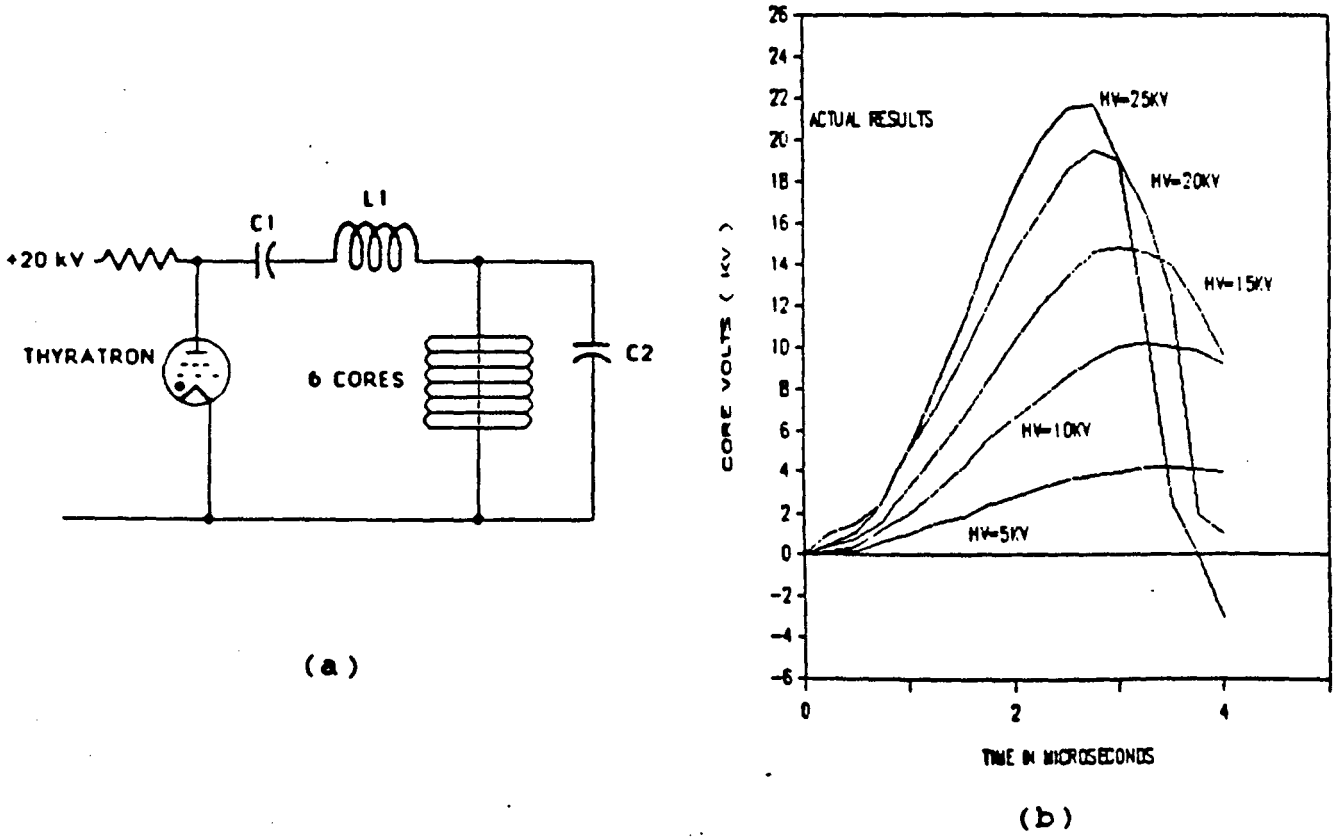

Figure 7- (a) Circuit used to produce accelerating waveforms for MBE4 and (b)) actual core voltages for various charge voltages.[3]

This requires that an operator must continually watch and "tune" the waveform for each gap. The third disadvantage of a summed pulser configuration is that it has not been tested at the voltage and current levels required for the ILSE gaps. The pulsers used on MBE4 were only required to produce gap voltages on the order of 30 KV. The thyratron switches would have to be replaced with spark gaps. The major advantage of the summed pulser configuration is that it has worked in the past and does not rely on any state of the art development projects in order for its chances of success to be reasonable. In addition, this configuration inherently has the ability to add the ears to each end of the gap waveform. The costs for a system such as this are also known to be on the order of $65,000 per acceleration gap. This cost per gap is considered to be reasonable and will be used as a standard for comparison of other pulser configurations.

3.3 Pulse Forming Line (PFL)

Another alternative pulser design that is used quite frequently in modern pulsed power systems is the Pulse Forming Line (PFL). The function of the PFL is exactly what the name implies; the pulse is formed when a specified transmission line is charged to an initial voltage and then discharged into a load which is matched or, as in this case, mismatched to the characteristic impedance of the transmission line. The characteristic impedance of a lossless transmission line is given by the equation:

$$Z = \sqrt{L/C} \qquad (1)$$

If a lossless transmission with a characteristic impedance Z is charged to an initial voltage V_o and discharged into a resistive load R_1 which is equal to Z at time t=0, the load voltage as a function of time will be as shown in figure 8a. Notice that the pulse in figure 8a is a single rectangular pulse which has a maximum amplitude of $V_o/2$ and a duration T=2d where d is the one way transit time of the transmission line given by the equation:

$$d = \sqrt{LC} \qquad (2)$$

The effect of mismatching the transmission line of figure 8d can be seen in figures 8b and 8c. Notice in particular the stepwise approximation to a negatively sloped ramp that the voltage in figure 8b makes. Since the load impedance of the cores to be used for ILSE is relatively constant with time you could ask the question: What would be the result of a changing transmission line impedance? Another way of looking at it would be to ask: Can the impedance of a lossless transmission line be designed such that pulses similar in shape to those desired for the ILSE pulsers can be produced?

If a ramp is to be produced by a single transmission line the first part of the pulse in time will be produced by the end of the transmission line that is closest in position to the load and the parts of the pulse later in time are produced by sections of the transmission line that are further and further away from the load. The load voltage at times close to t=0 are much smaller than the initial charge voltage on the transmission line so the line impedance must be much larger than the load impedance. For the purpose of assessing the feasibility

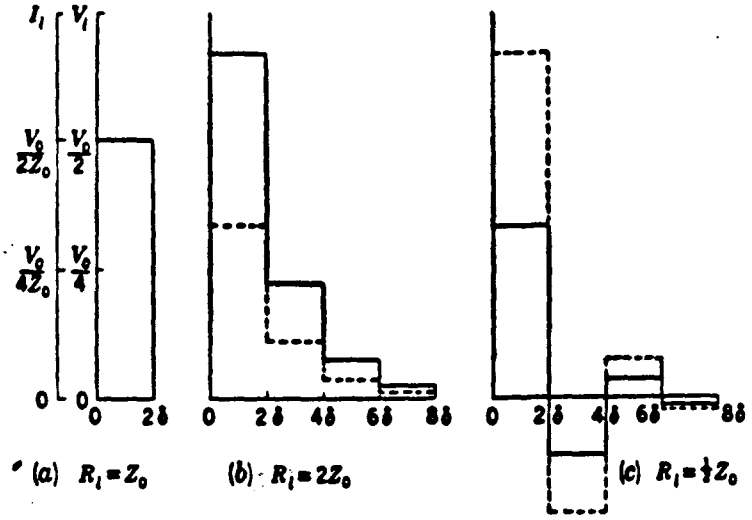

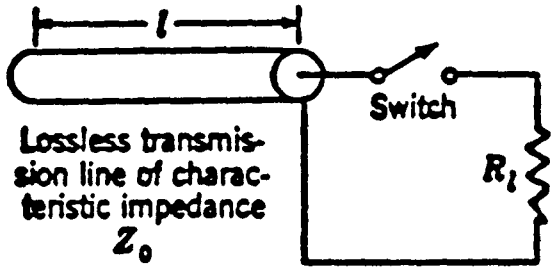

(d)

Figure 8- (a,b,c) Current and voltage pulses for a lossless transmission line (d) discharging into a resistive load. The solid and broken lines represent the voltage and current, respectively.[4]

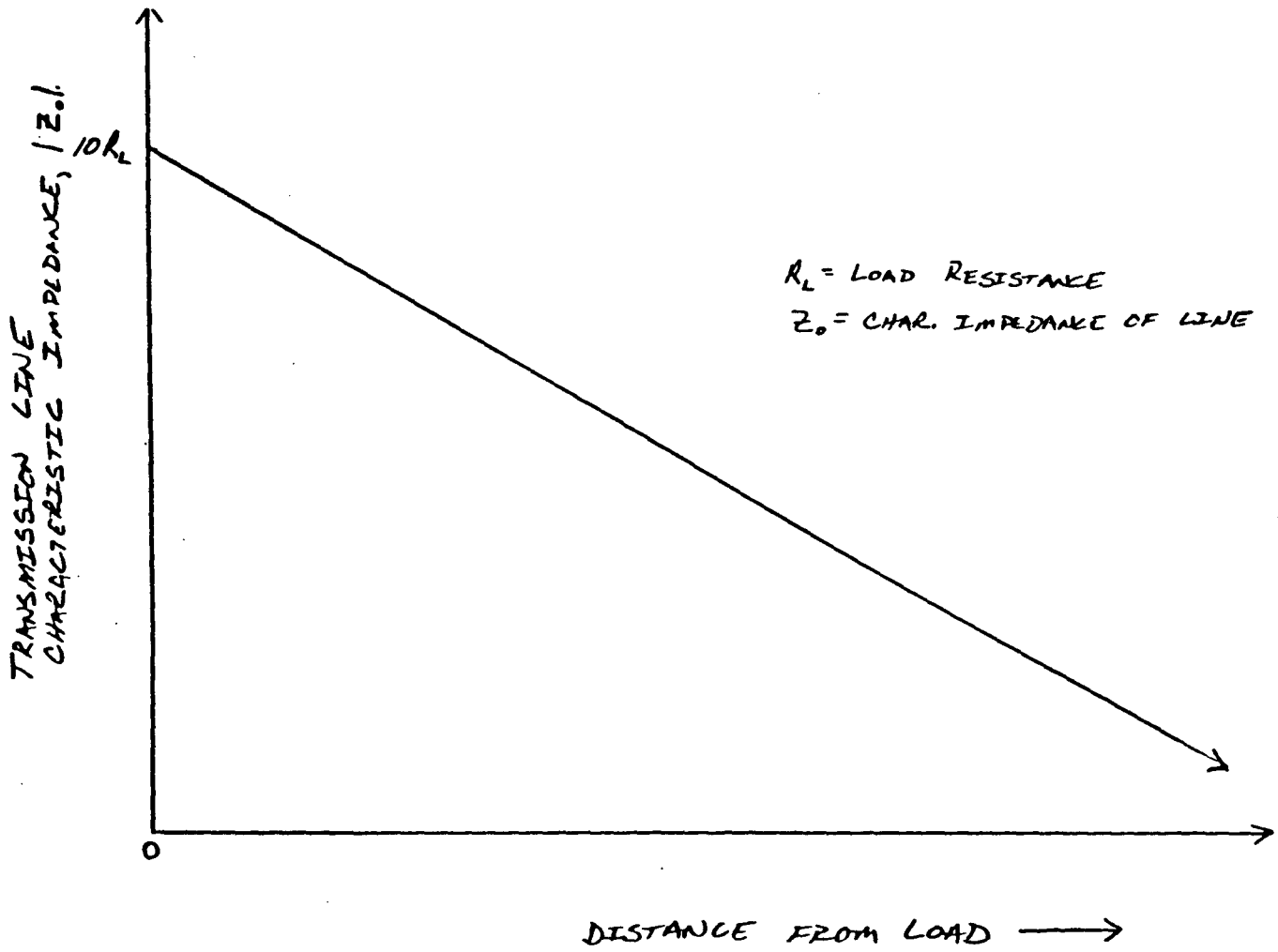

Figure 9- Possible characteristic impedance function of a Pulse Forming Line for use on ILSE.[9]

of this it idea was assumed that the ratio of the initial line impedance to the load impedance should be at least 10 to 1 (see figure 9). As you move further down the transmission line this ratio should decrease, eventually reaching a point where the line impedance is much less than the load impedance. Using a coaxial transmission line as a model the dimensions of this type of transmission line can be calculated.

The capacitance per meter and inductance per meter of coax are given in equations 3 and 4, respectively, where r_a and r_b are as shown in figure 10.

$$C = \frac{2\pi\epsilon}{\ln(r_b/r_a)} \quad F/m \tag{3}$$

$$L = \frac{\mu \ln(r_b/r_a)}{2\pi} \quad H/m \tag{4}$$

If equations (3) and (4) are substituted into equation (1), the characteristic impedance of the PFL can be expressed in terms of the dimensions of the coaxial cable. This was done and a linearly increasing impedance such as that shown in figure 9 was assumed. When realistic dimensions, dielectric constants and energy transfer efficiencies are assumed, the dimensions (outer radius and length) of this type of coaxial line become extremely large and unrealistic. This type of pulser was not pursued any farther.

3.4 Pulse Forming Networks (PFN)

The Pulse Forming Network (PFN) is a lumped element approximation to a transmission line. The PFN serves the dual purpose of storing the energy required for a single pulse and discharging this energy into the load in the form

of a pulse of specified shape. PFN's in which the energy is stored in capacitances are referred to as voltage fed networks while networks employing inductive energy storage are referred to as current fed networks. Voltage fed networks are used almost exclusively because suitable opening switches needed for inductive energy storage are still not available. The major advantage that PFN's have to offer over other pulser configurations is that only the amount of energy required for each pulse is stored in the network. Another advantage of PFN's is that the networks are constructed of passive components only, other than the switches which would be necessary in virtually any pulser configuration. There have been many attempts to generate pulses from lumped parameter equivalents of transmission lines, but most met with only limited success until Guillemin developed his theories in the 1940's. In his paper "A Historical Account of the Development of a Design Procedure for Pulse Forming Networks", Guillemin outlines the procedure by which one would go about designing a PFN for a given application [4]. In this paper he also describes the methods for obtaining, and the advantages and disadvantages of the five types of PFN's shown in figure 10; but Guillemin only applied his theories to PFN's that generate rectangular pulses and thus far no one has developed any theories that cover the generation of non-rectangular pulses with PFN's. The following is a detailed discussion and presentation of the methods that have been developed during the course of this project, for designing Pulse Forming Networks that produce pulses that are not necessarily rectangular in shape.

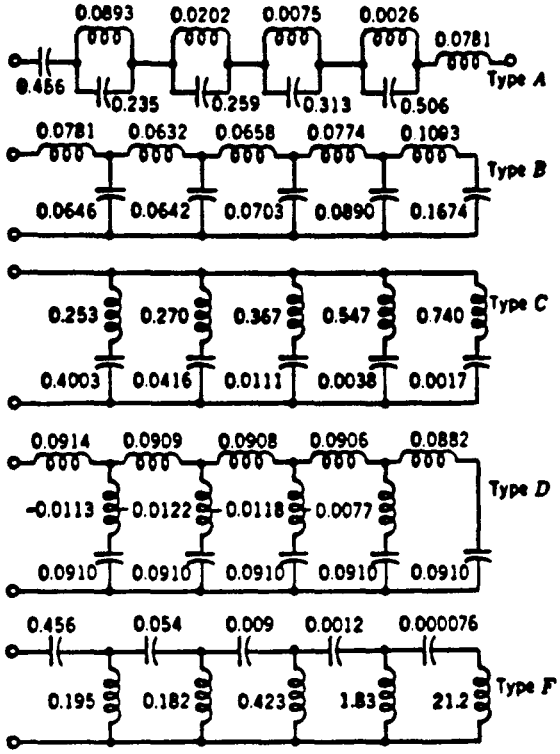

Figure 10- Equivalent forms for five-section Guillemin voltage- fed network.[4]

4.0 PULSE FORMING NETWORKS FOR NON-RECTANGULAR PULSES

4.1 Fourier Series of Continuous Waveforms

In general, any continuous, periodic, finite function can be expressed by an infinite sum of sine and cosine functions in the form of equation (5) below

$$f(t) = \frac{a_0}{2} + \sum_{n=1}^{\infty} \left(a_n \cos \frac{n\pi t}{\tau} + b_n \sin \frac{n\pi t}{\tau} \right) \tag{5}$$

where a_n and b_n are given by:

$$a_n = \frac{1}{\tau} \int_{-\tau}^{\tau} f(t) \cdot \cos \frac{n\pi t}{\tau} \, dt \tag{6a}$$

$$b_n = \frac{1}{\tau} \int_{-\tau}^{\tau} f(t) \sin \frac{n\pi t}{\tau} \, dt \tag{6b}$$

This infinite sum of sine and cosine terms is called the Fourier series of the function f(t) [5].

4.2 The Simple L-C Circuit

The simple series L-C circuit of figure 11a has a steady state current response given by the equation:

$$i(t) = v_c(0^-) \sqrt{\frac{C}{L}} \cdot \sin\left(\frac{t}{\sqrt{LC}} \right) \tag{7}$$

where vc(0-) is the initial charging voltage on the capacitor. If a small load resistor is added to the circuit as shown in figure 11b, the steady state current response of the circuit will be:

$$i(t) = \frac{v_c(0^-)}{L} \left(\frac{1}{LC} - \frac{R^2}{4L^2} \right)^{-1/2} e^{-\frac{R}{2L}t} \sin\left[\left(\frac{1}{LC} - \frac{R^2}{4L^2} \right)^{1/2} t \right] \tag{8}$$

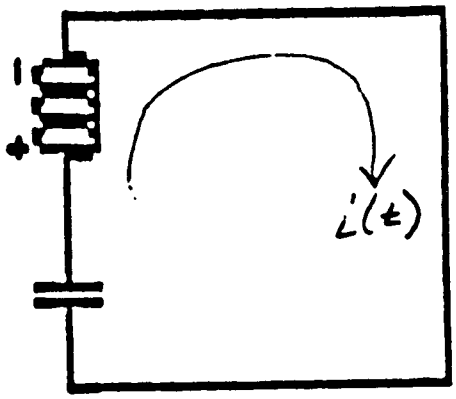

$$i(t) = v_{C_n}(0^-)\sqrt{C/L}\ \sin\left(t/\sqrt{LC}\right)$$

(a)

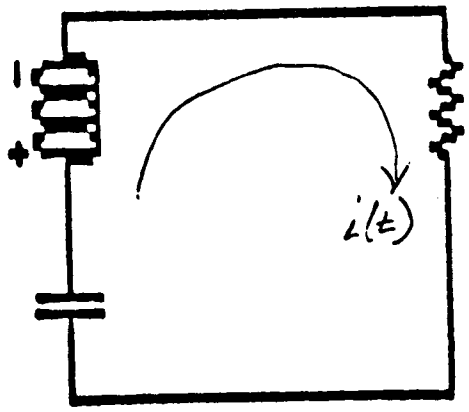

$$i(t) = \frac{v_{C_n}(0^-)}{L}\left(\frac{1}{LC} - \frac{R^2}{4L^2}\right)^{-1/2} e^{-\frac{R}{2L}t} \sin\left[\left(\frac{1}{LC} - \frac{R^2}{4L^2}\right)^{1/2} t\right]$$

(b)

Figure 11- (a) Simple L-C circuit. (b) L-R-C circuit.

The steady state voltage across the resistor will then be:

$$v(t) = i(t) \cdot R$$, where i(t) is given by eqn. (8). (9)

The introduction of the resistor to the circuit has now changed the steady state current response from a simple oscillatory function of one frequency to a damped oscillatory function of a different frequency. The equation has not only changed in form, but also in complexity, but if it is assumed that the value of the resistance is small when compared to L in equation (8), equation (7) can be used to approximate the steady state current through the resistor and the voltage across the resistor can be approximated by equation (10).

$$v(t) = R \cdot v_c(0^-)\sqrt{C/L} \cdot \sin\left(\frac{t}{\sqrt{LC}}\right) \qquad (10)$$

This result will be used in the following sections.

4.3 Pulser Synthesis for a Ramp Waveform

In order to synthesize a network that will produce a ramp waveform of the form shown in figure 2, the fourier series for the waveform must be known. The transient waveform of figure 2 must therefore be converted into a continuous periodic function. There are two choices, illustrated in figures 12a and 12b, that make the calculation much simpler. In figure 12a the desired ramp waveform is shown in the form of a even continuous periodic function. Because of the nature of the definition of a_n and b_n, b_n will be zero for all even functions. The opposite is true for the odd function of figure 12b. For the purpose of

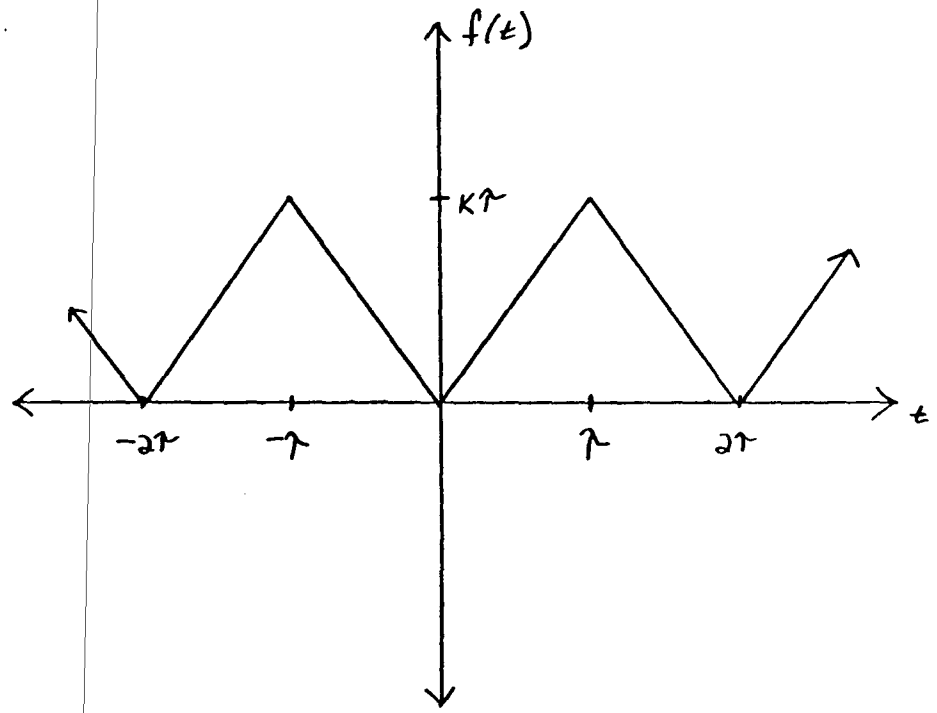

(a)

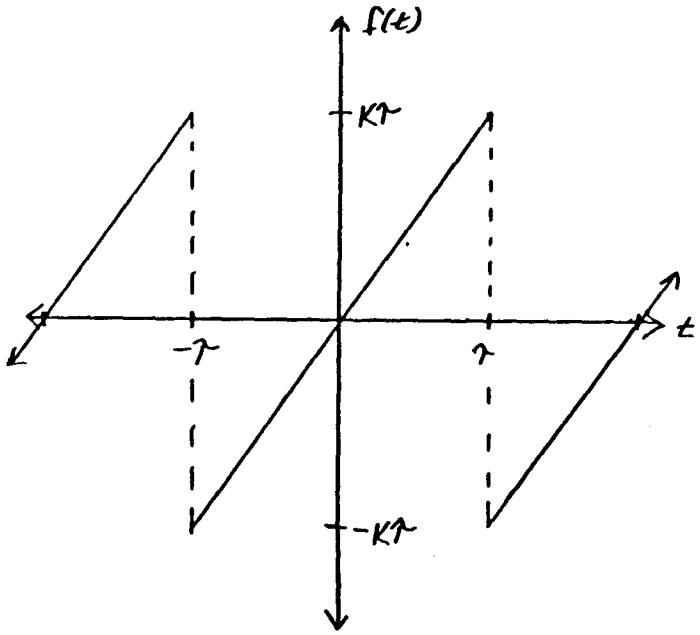

(b)

Figure 12- ILSE ramp waveform shown as: (a) a continuous, periodic, even, and (b) a continuous, periodic, odd function of time.

convenience the odd function of figure 12b was chosen from which to develop the fourier series for a ramp function. The reasons for this will become clear in later sections.

If equation 6b is solved for the waveform of figure 12b an expression for b_n can be obtained.

$$b_n = \frac{2K\tau}{n\pi}(-1)^{n+1} \tag{11}$$

Substituting this equation into equation (5), taking into account that all a_n terms are zero, leads to an expression for the even function of figure 12b given by:

$$f(t) = \frac{2K\tau}{\pi} \sum_{n=1}^{\infty} \frac{(-1)^{n+1}}{n} SIN\left(\frac{n\pi t}{\tau}\right) \tag{12}$$

Comparing this expression to the expression for the steady state voltage of equation (10) we get the equalities,

$$v_{cn}(0^-)\sqrt{C_n/L_n} = \frac{2K\tau R}{n\pi}(-1)^{n+1} \tag{13}$$

and,

$$\frac{1}{\sqrt{L_n C_n}} = \frac{n\pi}{\tau} \tag{14}$$

If we then solve these equations for L_n and C_n we get,

$$L_n = \tau/2 \tag{15}$$

and,

$$C_n = \frac{2\tau}{n^2\pi^2} \tag{16}$$

if

$$v_{cn}(0^-) = RK\tau(-1)^{n+1} \tag{17}$$

These expressions for L_n, C_n, and $v_{cn}(0-)$ lead to a network of the form of figure 13, where the values of the inductors, capacitors and initial charging voltage on the capacitors are given by equations (15), (16), and (17), respectively. Note that the odd harmonic capacitors are initially charged to a positive voltage while the even harmonics are initially charged to a negative voltage of the same magnitude.

4.4 Pulser synthesis for a trapezoid waveform

Using the procedure outlined above for the ramp waveform as a guide, a network that will produce a trapezoid waveform similar to that shown in figure 2 can be synthesized. The first step in the process is to convert the transient waveform of figure 2 to a continuous periodic function. Figures 14a and 14b show two possible choices. Figure 14a representing an even function and 14b representing an odd function. In order to be consistent with the section above the odd function was chosen as the waveform from which to synthesize the network. The fourier series for the waveform of figure 14b is given by:

$$f(t) = \frac{a}{\pi}\sum_{n=1}^{\infty}\left[\frac{(-1)^{n+1}}{n} + \frac{\pi}{n}\right] K\tau \cdot \sin\left(\frac{n\pi t}{\tau}\right) \tag{18}$$

Comparing this equation to equation (10) leads to the following equalities.

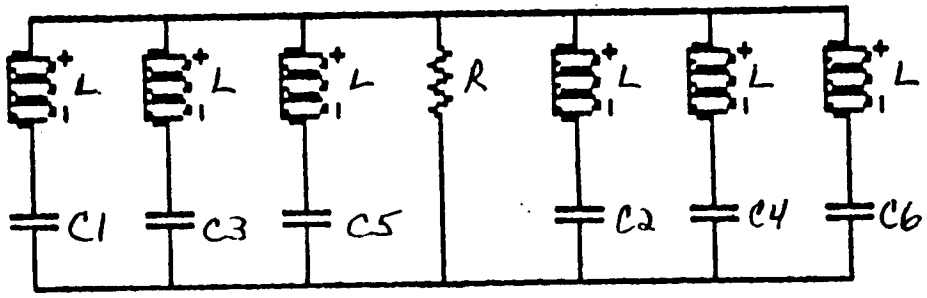

$$L_n = \tau/2$$

$$C_n = 2\tau/n^2\pi^2$$

$$v_{C_n}(0^-) = RK\tau(-1)^{n+1}$$

Figure 13- Bi-Polar, Guillemin type C network synthesized from fourier series for the odd function of figure 12b.

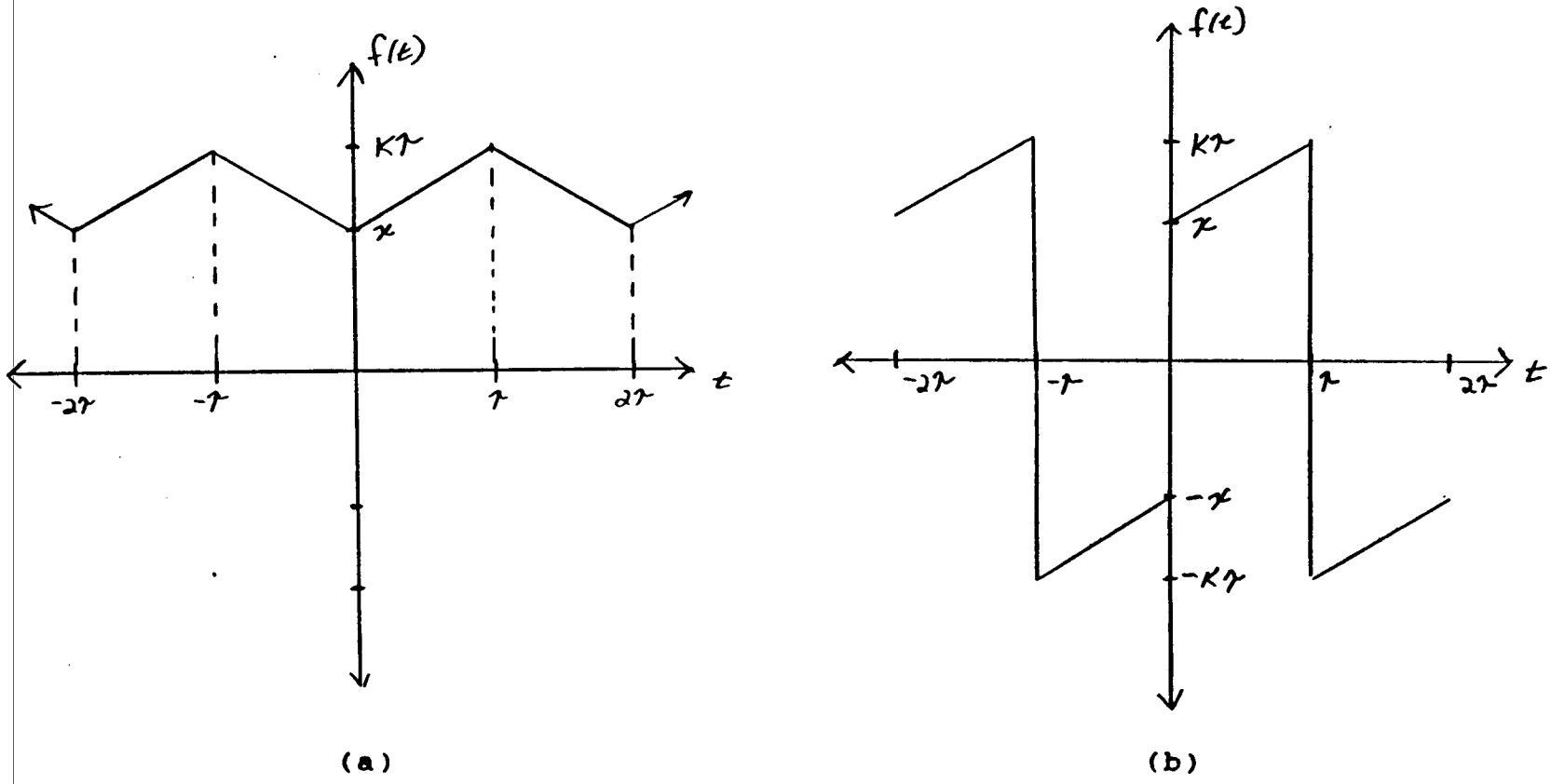

Figure 14- ILSE trapezoid waveform shown as: (a) a continuous, periodic, even, and (b) a continuous, periodic, odd function of time.

$$R\, v_{C_n}(0^-)\sqrt{C_n/L_n} = \frac{2}{\pi}\left[\frac{(-1)^{n+1}}{n} + \frac{n}{n}\right]K\uparrow \tag{19}$$

$$\frac{1}{\sqrt{L_n C_n}} = \frac{n\pi}{\uparrow} \tag{20}$$

Solving these equations for L_n and C_n leads to:

$$L_n = \frac{v_{C_n}(0^-)\cdot\uparrow}{2R\left[(-1)^{n+1}+n\right]K\uparrow} \tag{21}$$

$$C_n = \frac{2\uparrow\left[(-1)^{n+1}+n\right]RK\uparrow}{n^2\pi^2\, v_{C_n}(0^-)} \tag{22}$$

These two expressions look complex but can be simplified greatly if $v_{cn}(0\text{-})$ is allowed to defined according to equation (23).

$$v_{C_n}(0^-) = \left[(-1)^{n+1} + n\right]RK\uparrow \tag{23}$$

Equations (21) and (22) then reduce to:

$$L_n = \uparrow/2 \tag{24}$$

and,

$$C_n = \frac{2\uparrow}{n^2\pi^2} \tag{25}$$

Equations (24) and (25) are the same as equations (15) and (16). The implication of this being that the same network that is used to produce a ramp waveform can be used to produce a trapezoid waveform. The only difference is

that the initial charging voltages are given by equation (23) instead of equation (17).

4.5 Pulser synthesis for rectangular waveforms

The synthesis of Pulse Forming Networks that produce rectangular pulses has been well documented over the years. Guillemin even went so far as to publish normalized 1 ohm networks that can be impedance and time scaled to produce pulses of any duration and magnitude desired (see figure 10), so a duplication of effort is not necessary in this section. The point worth discussing is that a rectangular pulse is really just a trapezoid pulse in which both the initial voltage at t=0 (xKT in figure 14b) and the voltage at the end of the pulse (KT in figure 14b) are the same. Therefore all the equations developed in the preceding section for the trapezoid waveform can be used to synthesize a network that will produce a rectangle waveform. If x and KT are equal in equation (23) then,

$$v_{cn}(0\text{-}) = 0 \text{ for } n \text{ even.} \tag{26}$$

and

$$v_{cn}(0\text{-}) = 2KTR \text{ for } n \text{ odd} \tag{27}$$

This means that the even numbered sections in figure 13 can be omitted from the circuit. Intuitively this seems to be correct since the fourier series for a rectangular pulse contains only odd harmonics. The values of the capacitors and inductors for the odd numbered sections are still given by equations (25) and (24), respectively.

4.6 Summary of pulser synthesis

In summary, the network of figure 13 should be capable of producing all three types of pulsers required for ILSE. The values for the inductors and capacitors in the network are given by,

$$L_n = \frac{\tau}{2} \tag{28}$$

and,

$$C_n = \frac{2\tau}{n^2\pi^2} \tag{29}$$

and the initial voltages on the capacitors, $v_{cn}(0-)$, is given by,

$$v_{c_n}(0^-) = \left[(-1)^{n+1} + x\right] RK\tau \tag{30}$$

where x=0 for a ramp

x<1 for a trapezoid

x=1 for a rectangle.

5.0 COMPUTER SIMULATION

In order to test the validity of the equations derived above, computer simulations were performed. All computer simulations discussed in this section or any of the following sections were done on an IBM XT Personal Computer using the MICROCAP II simulation software package. The following is a summary of the results.

5.1 Ramp Waveform Simulation

Referring to figures 12b and 13 and substituting the values KT=T=R=1 into equations (28), (29), and (30) leads to the following values for the components in figure 13:

$$L1=L2=L3=L4=L5=L6=0.5 \text{ Henries} \tag{31}$$

$$C1=\ 0.2026\ F \quad C2=\ 0.05066\ F$$

$$C3=\ 0.02252\ F \quad C4=\ 0.01267\ F \tag{32}$$

$$C5=\ 0.00811\ F \quad C6=\ 0.00563\ F$$

$$v_{cn}(0\text{-})=\ 1.0, \text{ for } n=1,3,5$$

$$v_{cn}(0\text{-})=-1.0, \text{ for } n=2,4,6$$

Six harmonics were used in order to limit the number of components to a reasonable number. This limitation is valid since the contribution of each harmonic decreases as the square of the harmonic number. Guillemin investigated this point in his paper "A Historical Account of the Development of a Design Procedure for Pulse-Forming Networks", and the validity of this limitation has been documented in many publications since this paper [6]. Figure 15a shows the network with the values shown above and figure 15b is the computer predicted resistor voltage waveform for these values. The waveform depicted in figure 15b does approximate a ramp waveform as predicted with several notable exceptions;

1. Guillemin's theories for rectangular waveforms predict that the peak output voltage into a matched load should be one half the initial voltage

of the PFN. The waveform peak magnitude in figure 15b is roughly 0.5 volts while the initial differential PFN voltage is 2.0 volts. Therefore the network impedance is not 1 ohm.

2. The peak voltage occurs at approximately 0.8 seconds instead of 1.0 seconds as predicted. The sawtooth waveform used to derive the network approximation also had an infinitesimally small fall time following the voltage peak. The fall time for the tail of the pulse is approximately 250 nanoseconds.
3. The waveform in figure 15b has several ripples in the "linear" portion of the ramp. These are not predicted by the fourier derivation of the network.

These differences between theory and computer predictions are addressed in the following sections.

5.1.1 Peak amplitude differences

Transmission line theories and Guillemin theory which was derived from transmission line theory, both predict that the output peak voltage for a matched transmission line is one half of the initial voltage on the network. If these theories also apply to this type of "bi-polar PFN", the peak output voltage for the ramp waveform should be one half of the initial differential voltage on the network. The differential voltage is 2 volts in this case, therefore the peak voltage for the ramp should be 1 volt if the network is matched to the load. The peak in figure 15b is only 0.5 volts, which means that the network impedance is higher than 1 ohm (i.e. the voltage divider ratio of the network impedance and the load

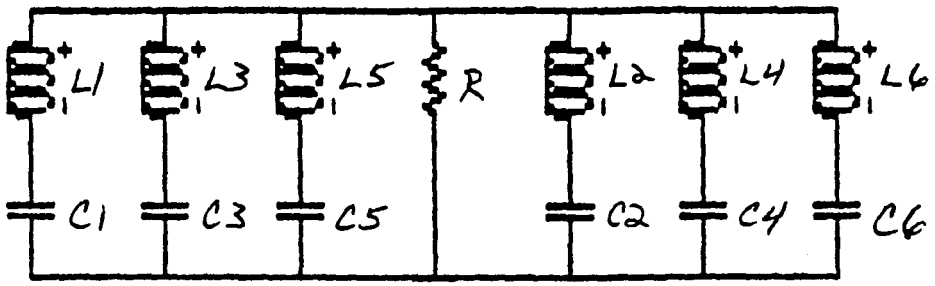

L1=L2=L3=L4=L5=L6=0.5 Henries

C1= 0.2026 F C2= 0.05066 F

C3= 0.02252 F C4= 0.01267 F

C5= 0.00811 F C6= 0.00563 F

$v_{cn}(0-)$= 1.0, for n=1,3,5

$v_{cn}(0-)$=-1.0, for n=2,4,6

(a)

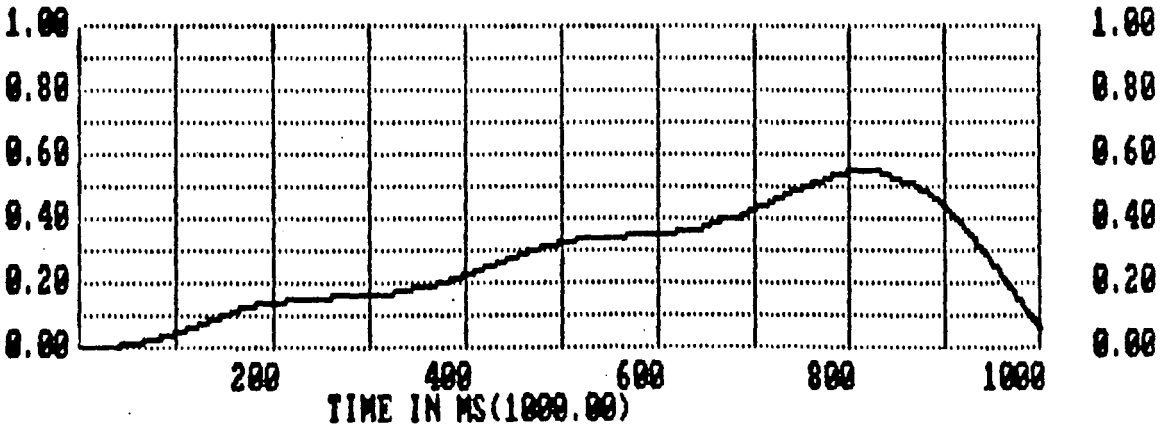

(b)

Figure 15- (a) Bi-Polar network synthesized to produce a 1 second, 1 volt ramp pulse. (b) Computer predicted output voltage waveform.

impedance is not correct). Equation (12) is the fourier series for the desired sawtooth waveform. The first harmonic for this equation is:

$$f_1(t) = \frac{2KT}{\pi} \sin\left(\frac{\pi t}{T}\right) \tag{33}$$

In the case at hand, KT=T=1, therefore equation (33) simplifies to:

$$f_1(t) = 0.6366 \sin(\pi t) \tag{34}$$

This implies that the voltage divider ratio of the network impedance and the load resistance should be 0.6366. Equation (35) expresses this implication.

$$\frac{R_L}{R_L + Z_1} = 0.6366 \tag{35a}$$

where R_1 is load resistance and

$$Z_1 = \sqrt{L_1/C_1} = \sqrt{\frac{0.5}{0.2026}} = 1.571\,\Omega \tag{35b}$$

Solving equation (35a) for R_1 leads to a matching load resistance of 2.749 ohms. Figure 16 shows the computer predicted load voltage waveform produced for the network if the load resistance is increased to 2.75 ohms. The peak voltage of the waveform has increased to approximately 0.85 volts. A voltage transfer ratio, n_v, for the network can be defined as the peak voltage into the load divided by the initial voltage on the network. The voltage transfer ratio of this network terminated into a 2.75 ohm load would then be 0.85/2.0=0.425. The question could then be asked; what happens if the load resistance is increased to a value greater than the network impedance? Figures 17a and 17b answer this question.

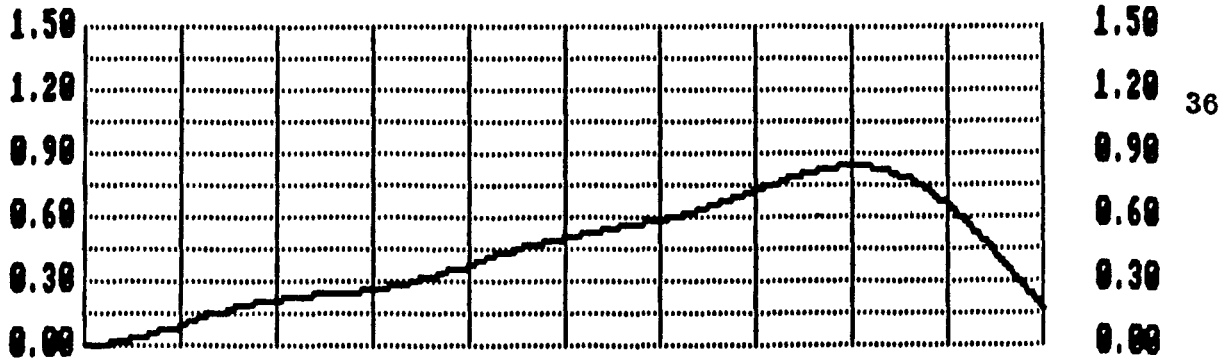

Figure 16- Computer predicted output voltage waveform for network of figure 15a terminated into a 2.75 ohm load resistance.

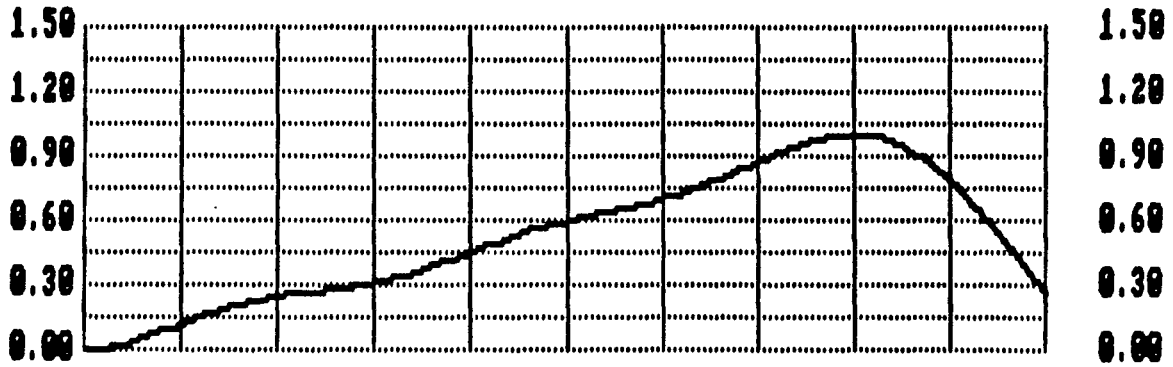

(a)

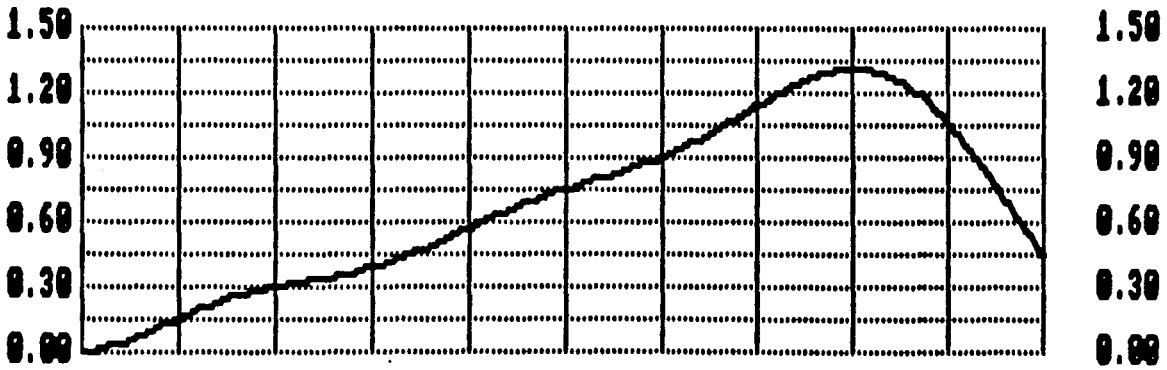

(b)

Figure 17- Computer predicted output voltage waveform for network of figure 15a terminated into (a) 5 ohms, and (b) 100 ohms.

The load resistances for these two figures are 5.0 and 100 ohms, respectively. Examination of figures 17a and 17b shows that the voltage transfer ratios are 0.51 and 0.65, respectively. Note that the shape of the waveform has remained essentially the same. The voltage transfer ratio in both cases has actually increased to a value greater than the 0.5 predicted for the matched PFN. This is also the case when a transmission line is terminated in a resistance that is greater in magnitude than its characteristic impedance. The next question is "If the voltage transfer ratio can be increased so easily, why not terminate the PFN in a resistance much larger than its characteristic impedance? ". The answer is simple. The major advantage that PFN's have over other types of pulsers is that virtually all the stored energy in the system is transferred to the load in a single pulse if the load and network impedances are matched. The increase in voltage transfer ratio has been obtained at the expense of energy transfer efficiency. This fact is born out by the plots of figure 18 which show the energy transfer efficiency n_e and the voltage transfer ratio n_v for various load resistances. Careful examination of figure 18 shows that the 2.75 ohm impedance calculated above is a good compromise between energy and voltage transfer efficiencies, but if either parameter is more important than the other, figure 18 can be used to see what penalty will be paid for an increase in one parameter at the expense of the other.

5.1.2 Peak voltage timing and ripples

The voltage peak for the ramp waveform occurs at approximately 0.8 seconds instead of the 1.0 seconds predicted by theory. Also, the fall time for the computer predicted waveform is not instantaneous and the linear portion of the ramp has several large ripples. These results show that lumped element networks

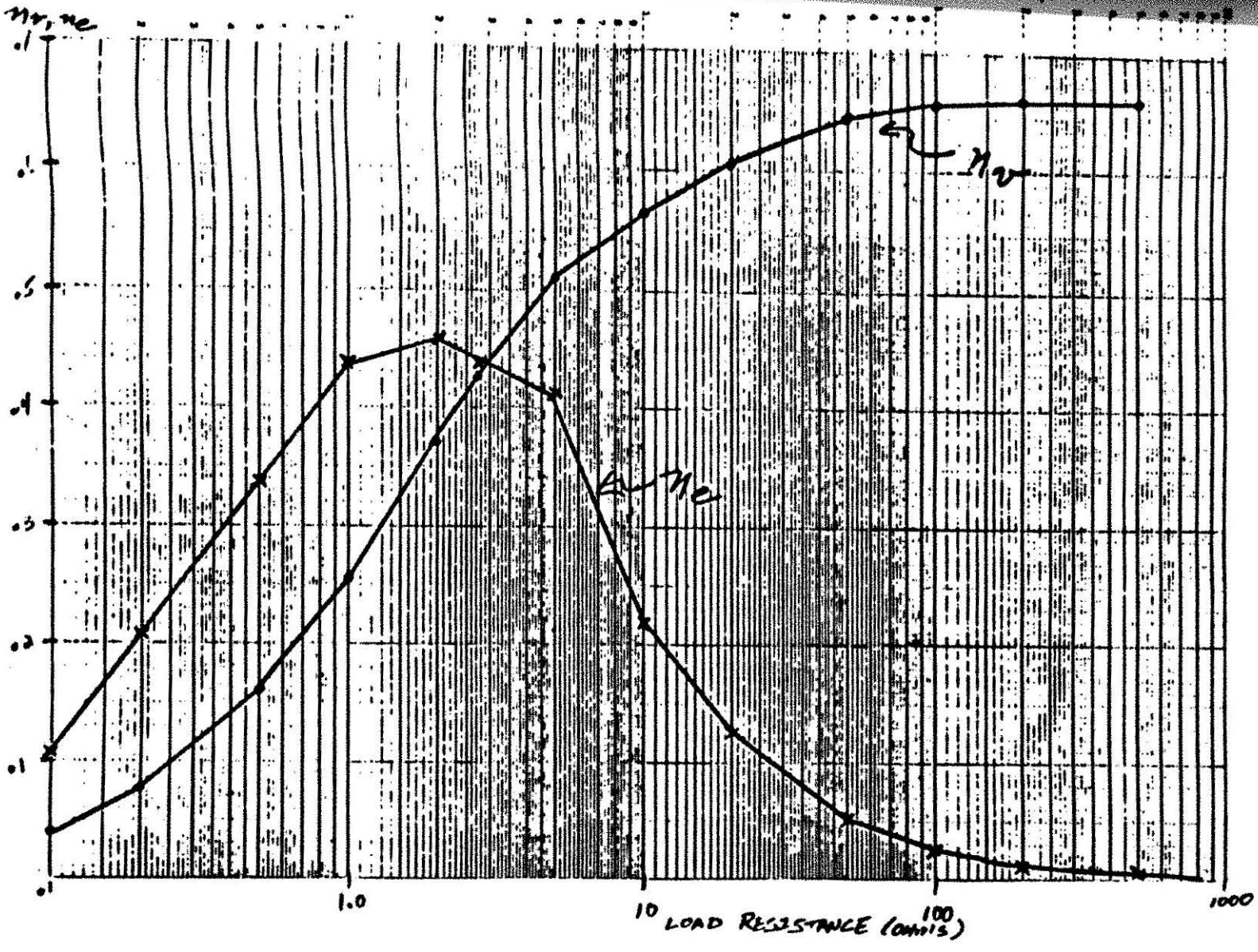

Figure 18- Voltage and energy transfer efficiencies for network of figure 15a versus load resistance.

used to simulate lossless transmission lines have limitations that are fundamental in nature. Gibbs correctly diagnosed these limitations as the results of an attempt to simulate an infinite fourier series with a finite number of terms. These problems of ripple and finite rise and fall times are referred to as the "Gibbs phenomenon". The problem of finite fall time does not affect a network that is designed to produce a pulse for ILSE since the portion of the pulse after the peak occurs after the ion beam has passed the acceleration gap. The network of figure 13 can just be time scaled so that the peak occurs at the desired 1 second [7]. Figures 19a and 19b show the time-scaled network and the computer predicted output waveform for a load resistance of 2.75 ohms. As an interesting sidenote, figure 19c shows the output waveform for the network if the simulation is allowed to continue for 5 seconds. The waveform produced by the network is indeed a sawtooth function as shown in figure 12b, although the peak amplitudes do decrease with every cycle and the waveform oscillations eventually damp out.

The ripples seen in the linear portion of the waveform will be addressed in the sensitivity section of this report.

5.1.3 Normalized PFN for ramp pulses

The results of the preceding two sections can be used to produce a network that will produce a 1 volt peak amplitude ramp pulse into a 1 ohm resistor. This normalized 1 ohm, 1 second network is shown in figure 20a and the computer predicted output for initial voltages of +/-1 volt are shown in figure 20b. This network can then be time and impedance scaled to produce pulses, of any

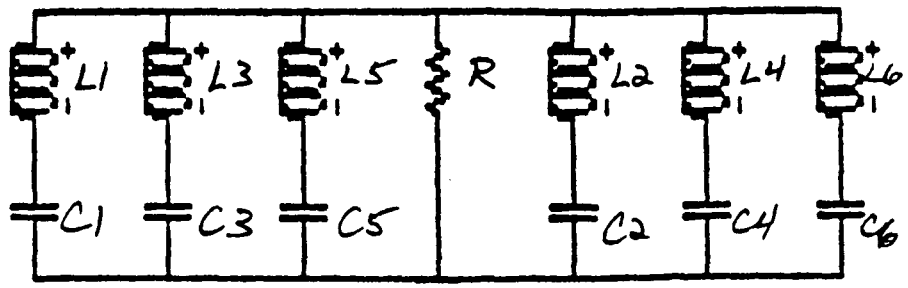

L1=L2=L3=L4=L5=L6= 0.625 Henries

C1= 0.2533 F C2= 0.0633 F

C3= 0.0281 F C4= 0.0158 F

C5= 0.0101 F C6= 0.0070 F

v (0-)= +1.0 volt, n=1,3,5

v (0-)= -1.0 volt, n=2,4,6

(a)

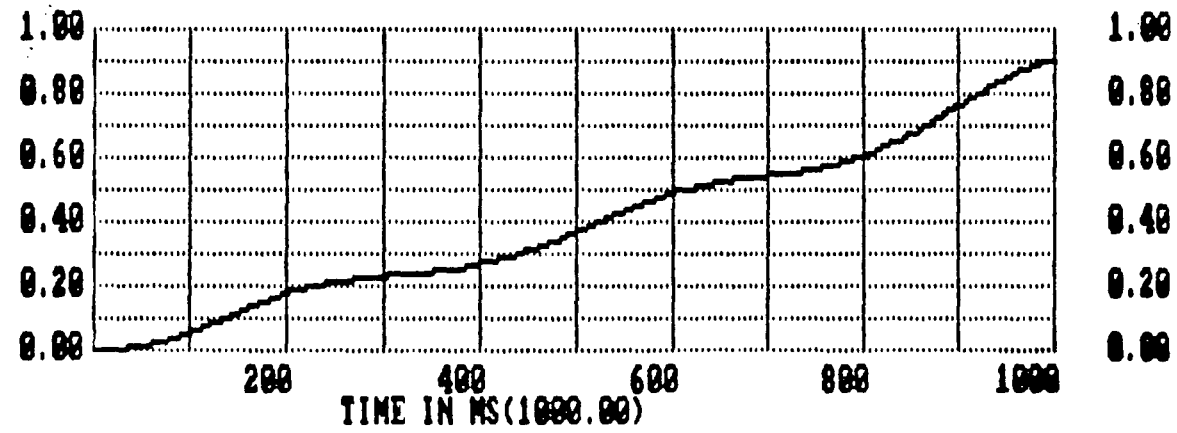

(b)

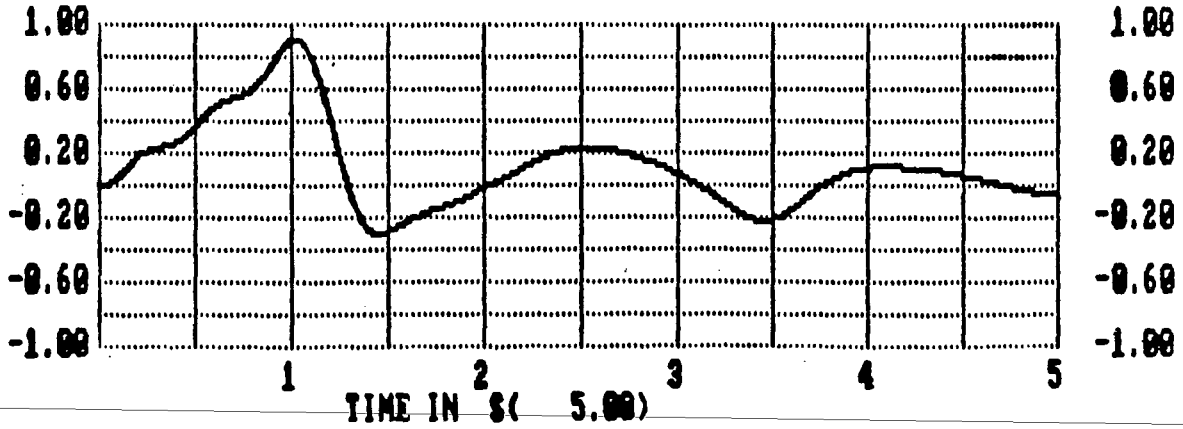

(c)

Figure 19- (a) Time-scaled bi-polar PFN. (b and c) Computer predicted output voltage waveforms.

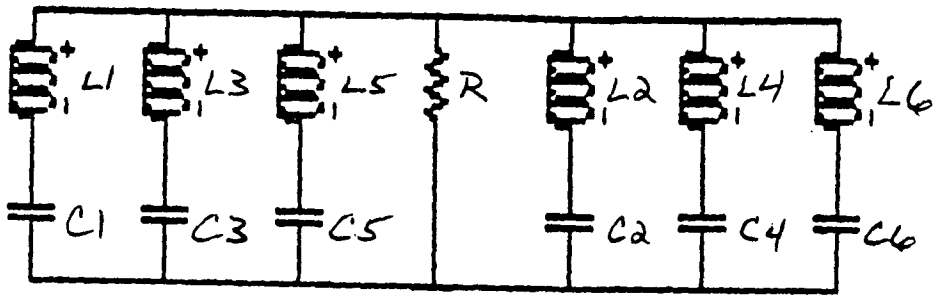

L1=L2=L3=L4=L5=L6= 0.227 Henries

C1= 0.6986 F C2= 0.1747 F

C3= 0.0776 F C4= 0.0437 F

C5= 0.0279 F C6= 0.0194 F

(a)

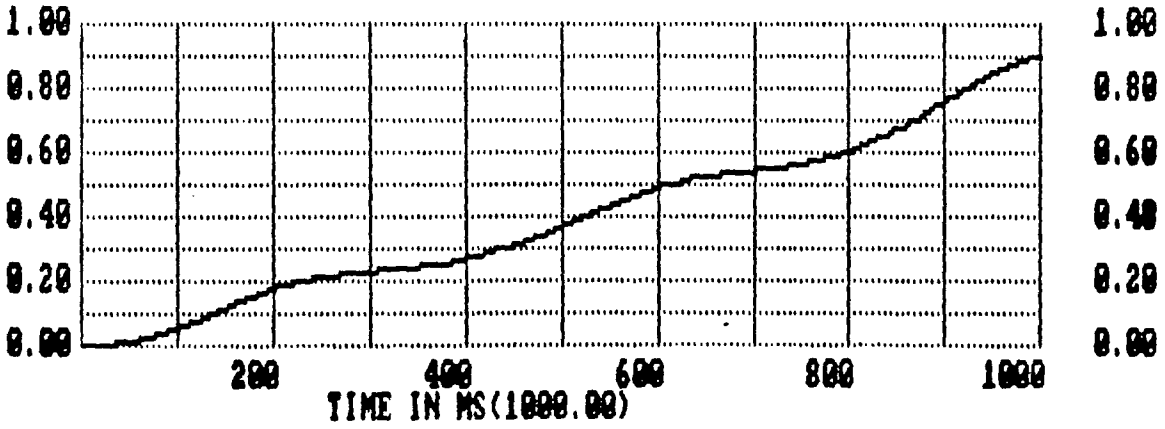

(b)

Figure 20- (a) Normalized bi-polar, one ohm, one second PFN used to produce ramp pulses. (b) Computer predicted output voltage waveform for odd and even initial capacitor voltages of +/- 1 volt, respectively.

duration into any resistance. The initial network voltages are given by equation (30).

5.2 Trapezoid waveform simulation

As a test of the validity of equations (28), (29), and (30), assume that a trapezoid pulse one second in duration, having an initial amplitude of 0.5 volts and peak amplitude of 1.0 volts is desired. Referring to figure 14b, this means that KT=T=1 and x=0.5. Substituting these values into equations (28), (29), and (30) leads to the same network as derived for the ramp pulse above (see equations 31 and 32), with the exception that the initial network voltages, $v_{cn}(0-)$ are given by:

$$v_{cn}(0-)=1.5 \text{ for } n=1,3,5 \qquad (36)$$
$$v_{cn}(0-)=-0.5 \text{ for } n=2,4,6$$

The network is shown in figure 21a. Since the value of 2.75 ohms proved to be a good compromise for ramp pulse described above, the matching load resistance R was initially assumed to be the same for the trapezoid pulse. The output waveform for the network into a 2.75 ohm load is shown in figure 21b.

As can be seen by examination of figure 21b the waveform produced by the network is a trapezoid pulse with an initial magnitude of 0.5 volts and a peak magnitude of approximately 1 volt. The ripples observed in the ramp pulse are also present in the trapezoid pulse and the pulse duration is only 800 milliseconds

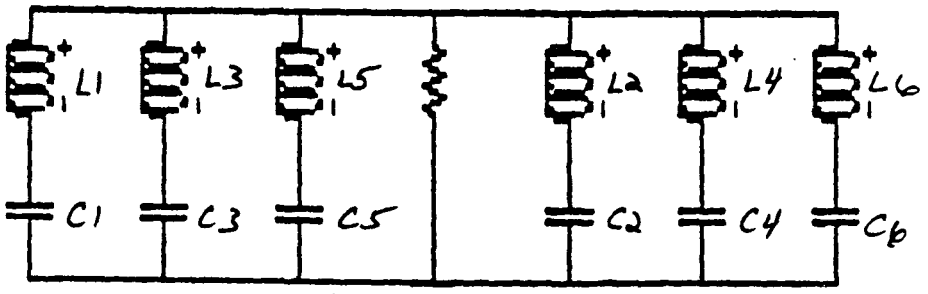

L1=L2=L3=L4=L5=L6=0.5 Henries

C1= 0.2026 F C2= 0.05066 F

C3= 0.02252 F C4= 0.01267 F

C5= 0.00811 F C6= 0.00563 F

v (0-)= +1.5 volt, n=1,3,5

v (0-)= -0.5 volt, n=2,4,6

(a)

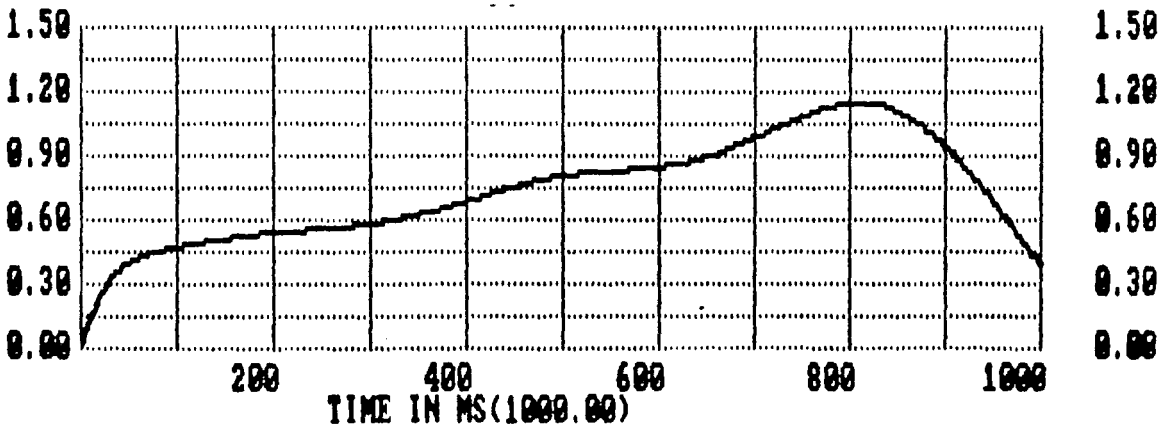

(b)

Figure 21- (a) Bi-polar network synthesized to produce a 1 second trapezoid pulse. (b) Computer predicted output voltage waveform for a 2.75 ohm load resistance.

instead of the predicted 1 second, but the 2.75 ohm resistor seems to provide a reasonable match for the network.

As was the case with the ramp pulse there is a trade-off of voltage transfer efficiency for energy transfer efficiency and vice-versa. This fact is born out by the plots of energy and voltage transfer efficiency versus load resistance shown in figure 22. It is interesting to note that the shapes of the curves are essentially the same as the curves in figure 18.

The premature occurrence of the peak magnitude can be handled by time scaling the network, as was done for the ramp pulse. This means that the time-scaled network of figure 19a can also be used for the trapezoid pulse and since the 2.75 ohm load resistance also provides a reasonable compromise in the trapezoid case the normalized network of figure 20a can be used to produce trapezoid pulses in addition to ramp pulses. For convenience the network is shown again in figure 23a. Figures 23b and 23c show the load voltage pulse for various initial network voltages.

5.3 Rectangular pulse simulation

Since the rectangular pulse is a special case of a trapezoid pulse, equations (28), (29), and (30) can be used to synthesize a network that produces a rectangular pulse of magnitude KTR and duration T. In equation (30), x would be equal to 1. This means that the charging voltages for all odd sections would be 2KTR and zero for all even sections. The zero initial voltage can be represented in two ways. The even numbered sections remain in the network but are

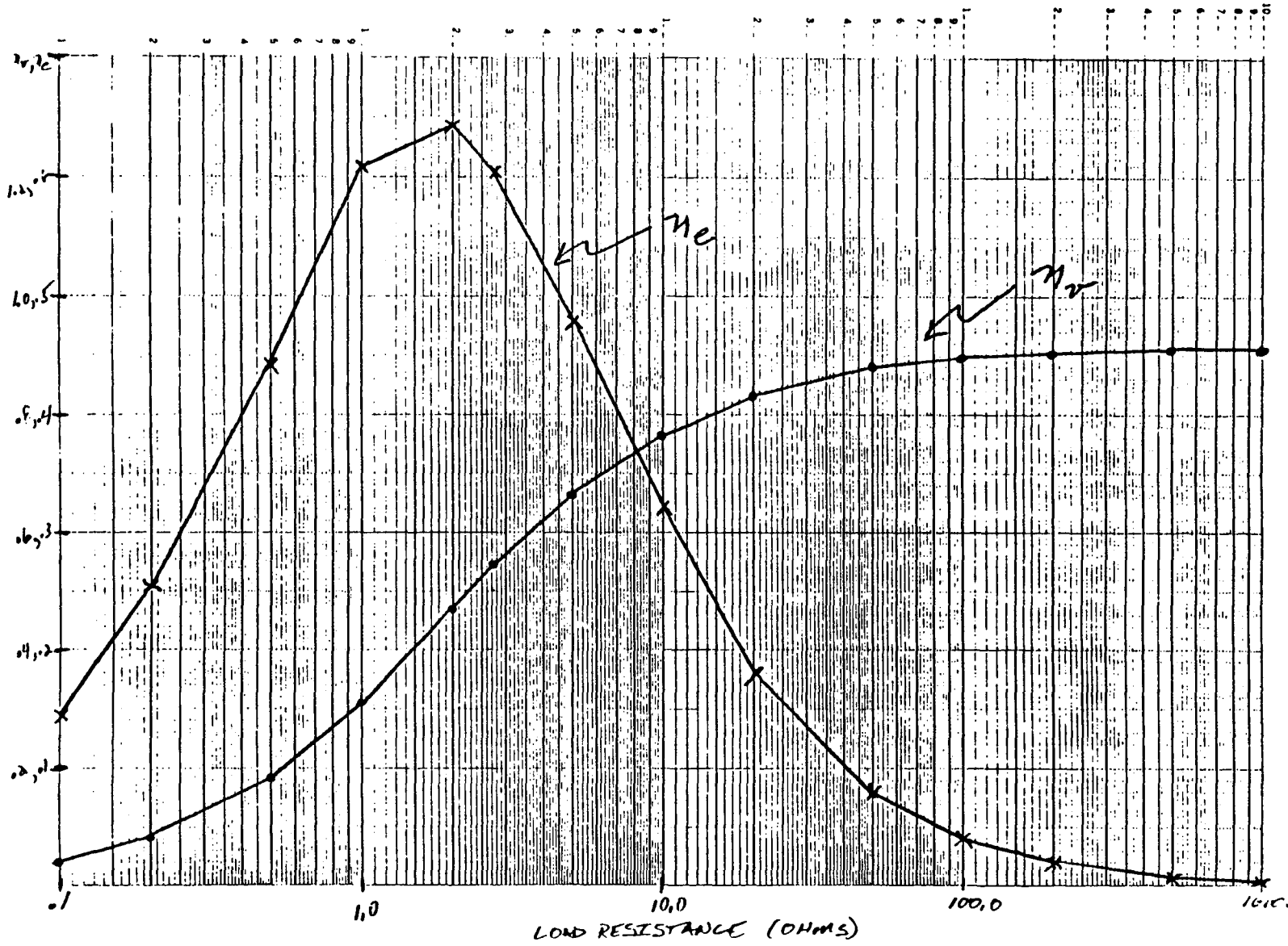

Figure 22- Voltage and energy transfer efficiencies versus load resistance for trapezoid network of figure 21a.

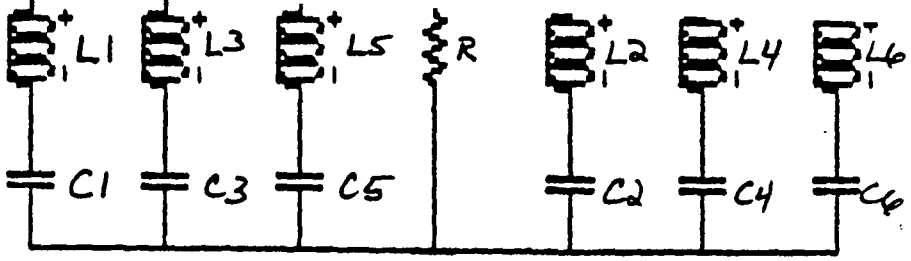

L1=L2=L3=L4=L5=L6= 0.227 Henries

C1= 0.6986 F C2= 0.1747 F

C3= 0.0776 F C4= 0.0437 F

C5= 0.0279 F C6= 0.0194 F

(a)

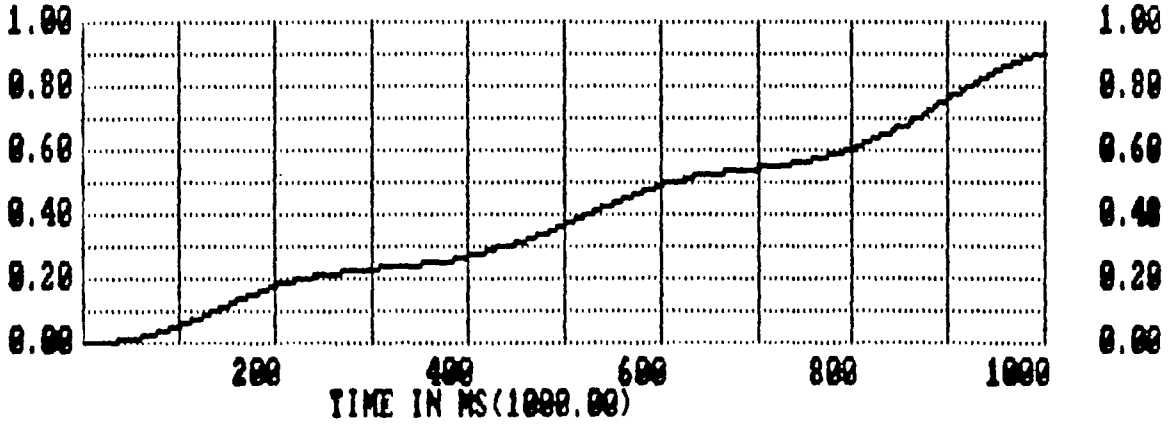

(b)

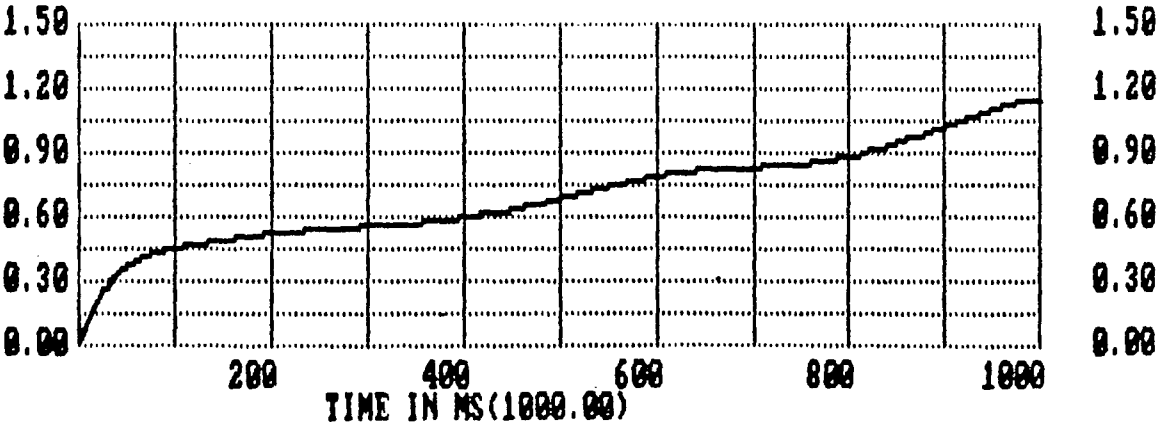

(c)

Figure 23- (a) Normalized, bi-polar, one ohm, one second PFN, and (b and c) computer predicted output voltage waveforms for various initial capacitor voltages.

initially uncharged or they can be deleted from the network altogether. Figures 24a and 24b show the computer predicted outputs for each of these cases when the load resistance is 2.75 ohms and initial voltages of 2 volts (odd sections only). The network component values were calculated using equations (28), (29) and (30) for KTR=T=1.0 (this yields the same network that was used for the ramp and trapezoid pulses above). Note that the waveform in figure 24a is not really a rectangle, but a trapezoid. The waveform of figure 24b, aside from the initial overshoot and ripples in the flattop portion of pulse, gives a closer approximation to the desired rectangle pulse. Intuitively, the deletion of the even numbered sections from the network makes sense since the fourier series of a rectangle waveform contains only the odd harmonic terms.

The overshoot at the beginning of the pulse can be attributed to what has come to be called the "Gibbs phenomenon". This behavior at points of discontinuity (i.e. zero risetime transition into flattop) is typical of fourier series approximations. Correction of this overshoot and the ripples during the flattop will be addressed in a later section.

Like the ramp and trapezoid pulses, the rectangle pulse of figure 24b terminates at 0.8 seconds instead of 1 second and, as before, the network can be time-scaled to accommodate.

Figure 25 shows the voltage and energy transfer ratios versus load resistance for the rectangular pulse case. The pulse voltage at 0.4 seconds was used to calculate nv. As was the case before, 2.75 ohms provides a reasonable compromise between

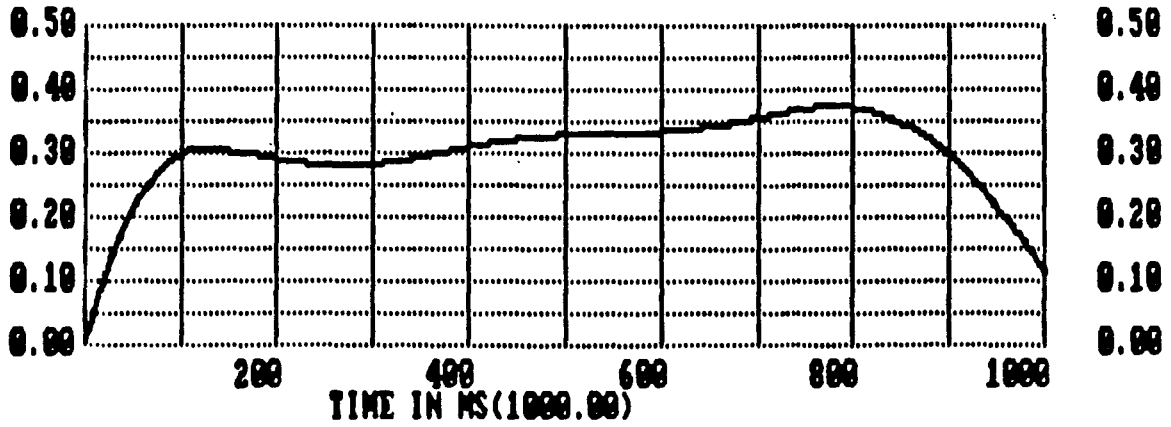

v (0-)= +1.0 volt, n=1,3,5

v (0-)= 0.0 volt, n=1,3,5

(a)

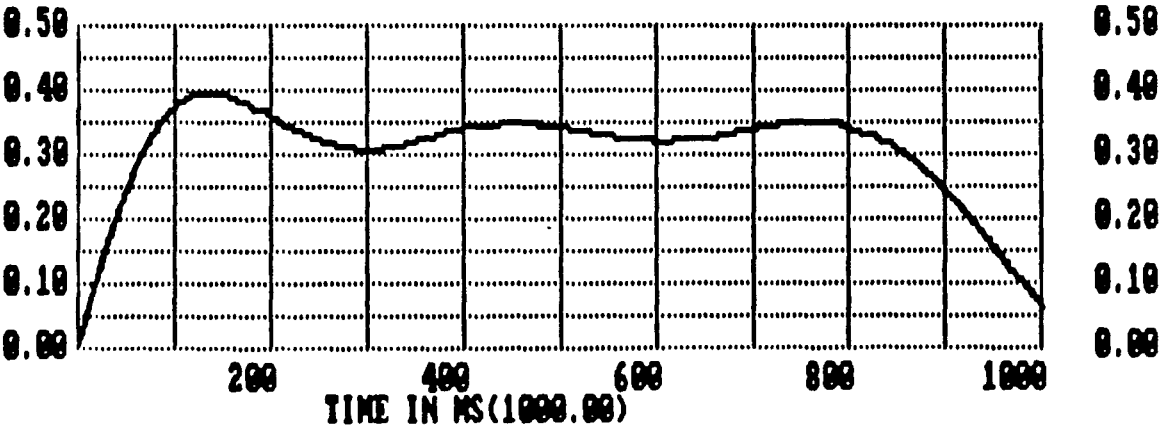

v (0-)= +1.0 volt, n=1,3,5

(b)

Figure 24- (a) Computer predicted output voltage waveform for the network of figure 15a. (b) Computer predicted output voltage waveform for network of figure 15a with even numbered (right side of load) sections removed. Initial capacitor voltages are as shown.

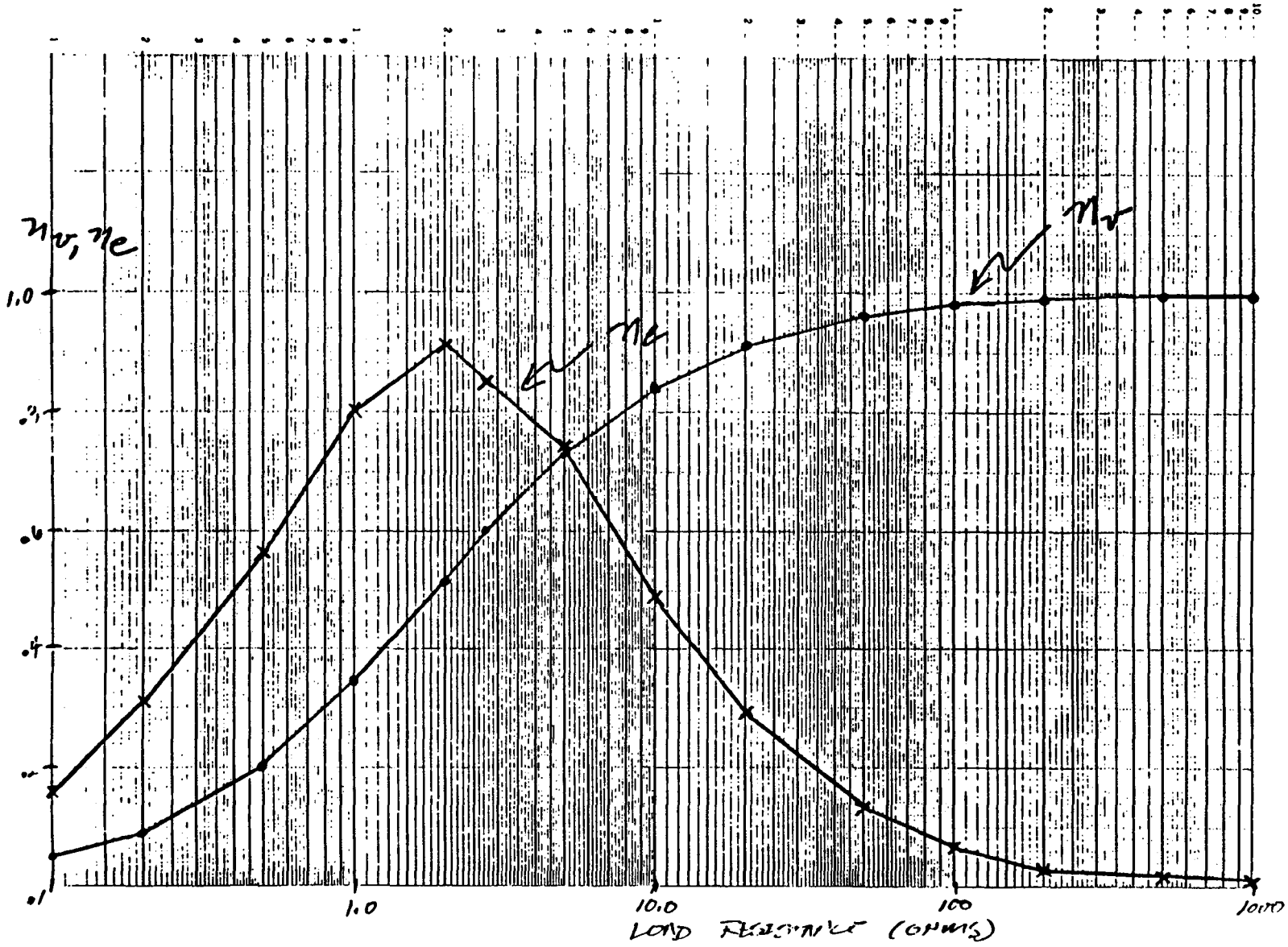

Figure 25- Voltage and energy transfer efficiencies versus load resistance for rectangular network of figure 24a (even sections removed).

energy and voltage efficiency. Therefore the normalized network of figure 23a, with the exception that the even numbered sections are deleted, can be used to produce rectangular pulses in addition to ramp and trapezoid. The conversion between the different types of pulses is accomplished by changing only the initial voltage on the odd and even sections with the initial voltages being determined by equation (30).

6.0 SENSITIVITY ANALYSIS

6.1 Sensitivity Analysis

In the real world the components used to fabricate a Pulse-Forming Network such as the one shown in figure 23a will not have exactly the same values as are required. The amount of the variation that can be tolerated will determine the accuracy to which the components must be fabricated. Prior knowledge of component tolerances can save many hours of heartache during initial testing in addition to saving many thousands of dollars during component fabrication. The standard way of determining the acceptable range of component variation is to perform a sensitivity analysis for each component in the network. The purpose of the sensitivity study is twofold. The first being to determine what affect component variations will have on the output voltage waveshape and magnitude. The second reason for performing the study is to obtain functions for each component in the network that may possibly be used to optimize, or tune the output waveform to something that more closely approximates the desired waveshape. The following is an explanation of the process used to perform the study and a summary of the results.

The sensitivity of a function G to a parameter p can be defined as,

$$S_p^G = \frac{\partial G}{\partial p} \cdot \frac{p}{G} \tag{37}$$

Equation (37) defines a relationship between the amount of change in a parameter p and the amount of change induced in the function G [8].

In an effort to simplify the sensitivity analysis of the output waveform function, the loading effects of each section of the network on any other section of the network were neglected. In addition the output current of the network into the resistive load was assumed to be a simple sum of the output currents of the individual L-C sections. This is a reasonable assumption since the matching load impedance is smaller than the impedance of each section of the network and therefore the load will carry most of the current. This simplified approximation for the total load current as a function of time is given by equation (38) below.

$$i(t) = \sum_{n=1}^{6} \frac{v_{C_n}(0^-)}{\sqrt{L_n/C_n}} \, SIN\left(\frac{t}{\sqrt{L_n C_n}}\right) \tag{38}$$

While an expression for the load current is important, the output voltage function is what is really needed. Since the load is assumed to be resistive, the expression for the output voltage as a function of time is:

$$v(t) = i(t) \cdot R = \sum_{n=1}^{6} \frac{v_{C_n}(0^-) R}{\sqrt{L_n/C_n}} \, SIN\left(\frac{t}{\sqrt{L_n C_n}}\right) \tag{39}$$

Sensitivity studies may be performed in the time or frequency domains. In order to work in the frequency domain you must first start with a expression for the output voltage as a function of s. The Laplace transform of equation (39) is:

$$V(s) = \sum_{n=1}^{6} \frac{v_{C_n}(0^-)R}{\sqrt{L_n/C_n}} \cdot \left[\frac{1/\sqrt{L_n C_n}}{s^2 - 1/L_n C_n} \right] \tag{40}$$

Using equation (37) as a guide, the sensitivity of the output voltage as a function of frequency to a variation in an inductor L_m is:

$$S_{L_m}^{V(s)} = \frac{\partial V}{\partial L_m} \cdot \frac{L_m}{V} \tag{41}$$

Solving equation (41) leads to:

$$S_{L_m}^{V(s)} = \frac{(L_m C_m)^2 s^2}{(L_m C_m s^2 - 1)^2} \cdot \left[\sum_{n=1}^{6} s^2 - \frac{1}{L_n C_n} \right] \tag{42}$$

In a similar manner, the sensitivity of the output voltage as a function of frequency to a variation in a capacitor C_m can be determined to be:

$$S_{C_m}^{V(s)} = \frac{-L_m C_m}{(L_m C_m s^2 - 1)^2} \cdot \left[\sum_{n=1}^{6} s^2 - \frac{1}{L_n C_n} \right] \tag{43}$$

Equations (42) and (43) can be used to determine the effects that varying values of inductors and capacitors will have on the frequency content of the output voltage waveform. Since most people have a hard time relating frequency domain changes to real time pulse shape and magnitude changes, it perhaps would be

more useful to determine the sensitivity of the waveform to component variations as a function of time.

Applying the definition of sensitivity to equation (39) leads to the following expressions:

$$S_{L_m}^{v(t)} = \frac{-\frac{1}{2}\sqrt{\frac{C_m}{L_m}}\left[\sin\left(\frac{t}{\sqrt{L_m C_m}}\right)+\left(\frac{t}{\sqrt{L_m C_m}}\right)\cos\left(\frac{t}{\sqrt{L_m C_m}}\right)\right](-1)^{m+1}}{\sum_{n=1}^{\infty}(-1)^{n+1}\left[\sqrt{C_n/L_n}\cdot\sin\left(\frac{t}{\sqrt{L_n C_n}}\right)\right]} \qquad (44)$$

$$S_{C_m}^{v(t)} = \frac{\frac{\frac{1}{2}C_m}{\sqrt{L_m C_m}}\left[\sin\left(\frac{t}{\sqrt{L_m C_m}}\right)+\left(\frac{t}{\sqrt{L_m C_m}}\right)\cos\left(\frac{t}{\sqrt{L_m C_m}}\right)\right](-1)^{m+1}}{\sum_{n=1}^{\infty}(-1)^{n+1}\left[\sqrt{C_n/L_n}\cdot\sin\left(\frac{t}{\sqrt{L_n C_n}}\right)\right]} \qquad (45)$$

where equation (44) is the sensitivity of the output voltage as a function of time for a changing L_m and equation (45) is the sensitivity of the output voltage as a function of time for a changing C_m. Close examination of equations (44) and (45) reveals that the denominator of each expression is the total load current i(t). Therefore, equations (44) and (45) can be rewritten as:

$$S_{L_m}^{v(t)} = \frac{\frac{-\frac{1}{2}(-1)^{m+1}}{\sqrt{L_m C_m}}\left[\sin\left(\frac{t}{\sqrt{L_m C_m}}\right)+\left(\frac{t}{\sqrt{L_m C_m}}\right)\cos\left(\frac{t}{\sqrt{L_m C_m}}\right)\right]}{i(t)} \qquad (46)$$

$$S_{C_m}^{v(t)} = \frac{\frac{\frac{1}{2}C_m(-1)^{m+1}}{\sqrt{L_m C_m}}\left[\sin\left(\frac{t}{\sqrt{L_m C_m}}\right)+\left(\frac{t}{\sqrt{L_m C_m}}\right)\cos\left(\frac{t}{\sqrt{L_m C_m}}\right)\right]}{i(t)} \qquad (47)$$

Figures 26 through 37 are plots of the sensitivity functions for each of the components in the normalized 1 ohm network of figure 23a. These plots show which parts of the output voltage waveform are affected by each component and it should be possible to use these plots to "tune out" the ripples that are observed in the normalized network output shown in figure 23b. The following is an attempt to do just that.

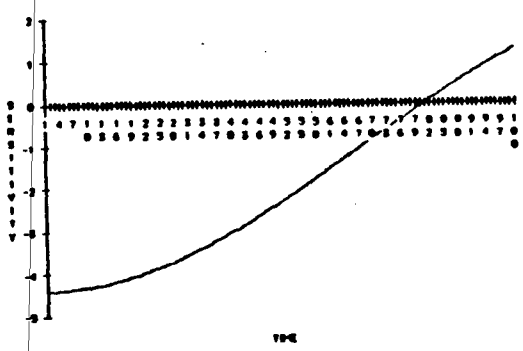

(26)

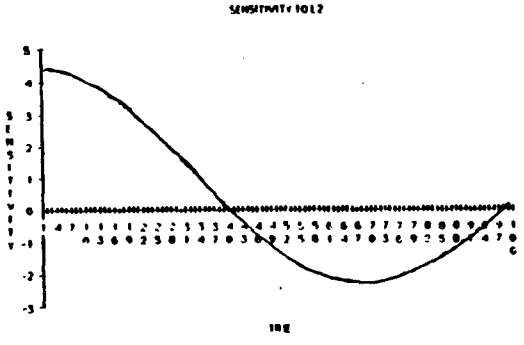

(27)

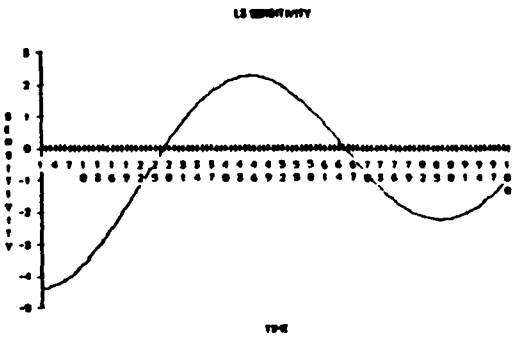

(28)

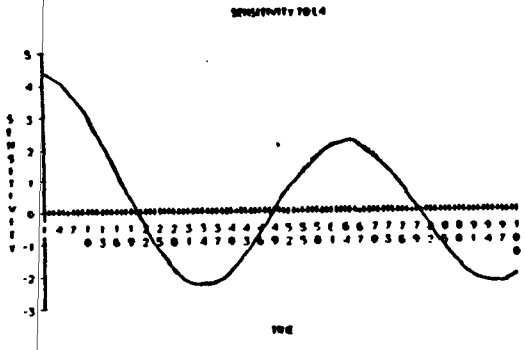

(29)

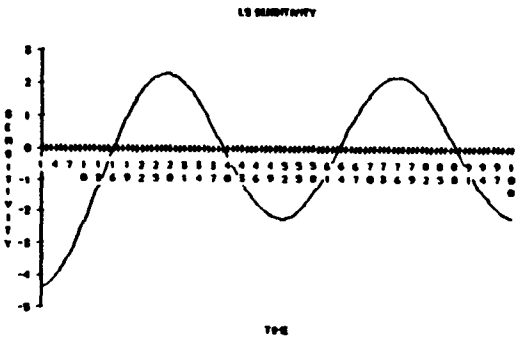

(30)

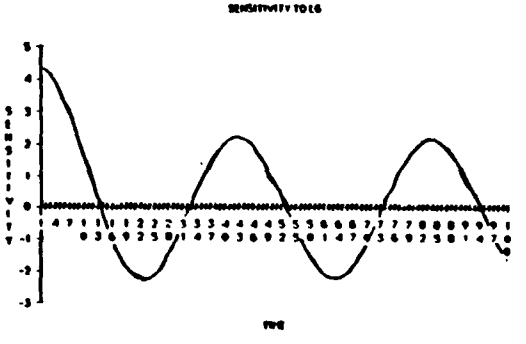

(31)

Figures 26 through 31- Simplified sensitivity functions for inductors L1 through L6 of figure 23a, respectively.

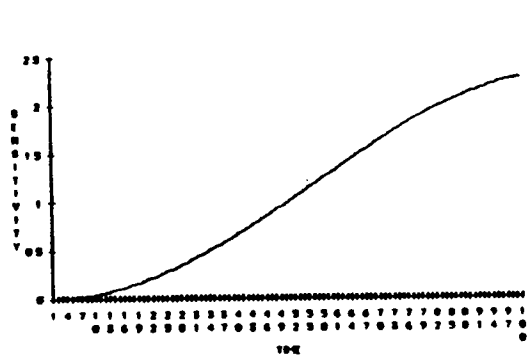

(32)

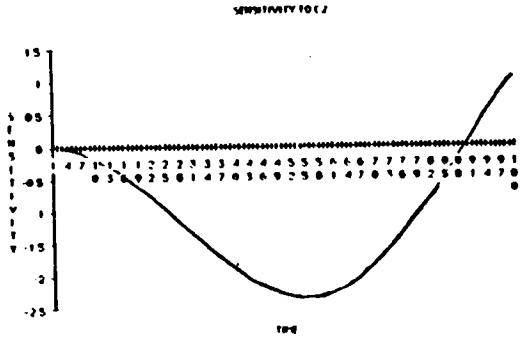

(33)

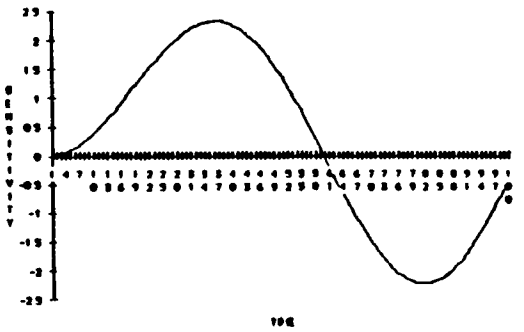

(34)

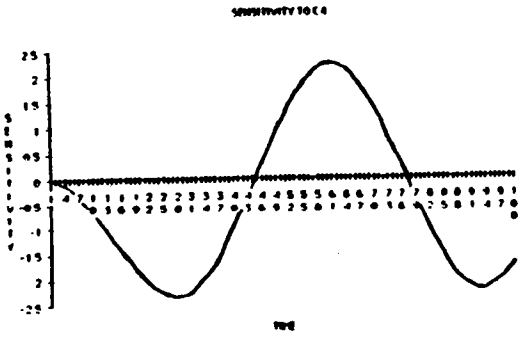

(35)

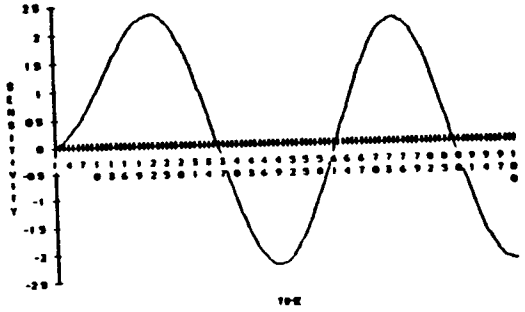

(36)

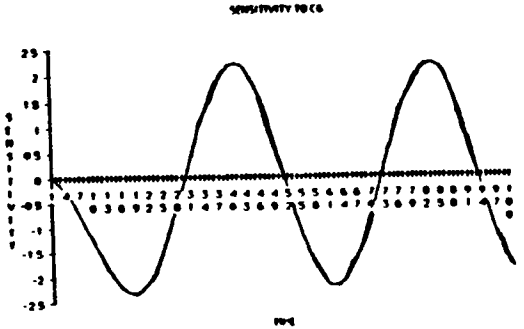

(37)

Figures 32 through 37- Simplified sensitivity functions for capacitors C1 through C6 of figure 23a, respectively.

6.2 Tuning with sensitivity plots

Notice that the waveform of figure 23b has positive ripple peaks at approximately 0.25, 0.63, and 1.0 seconds. The sensitivity plot for a change in C6 (figure 37) has negative ripple peaks at approximately the same points in time. This means that an increase in the value of C6 will result in a decrease of the output voltage at these points in time. Figure 38a is the computer predicted output for the network when C6 is increased by 20%. Comparison of the waveforms of figures 23b and 38a shows that the ripples have virtually vanished leaving a broad "dip" in the ramp from 0.4 to 0.9 seconds. The plot of the sensitivity to C2 (figure 33) has a broad negative peak in the same timeframe. Figure 38b is the computer predicted output for the network when C6 is increased by 20% and C2 is decreased by 20%. Notice that the dip has been eliminated by decreasing C2.

The same network is used to produce trapezoid pulses, therefore the sensitivity equations and plots derived above for ramp pulses can be used to tune trapezoid pulses. If the plot of the ramp pulse of figure 23b is compared to the trapezoid pulse of figure 23c, it becomes clear that the ripples in each waveform are in essentially the same places. If this is true the optimized network derived for the ramp pulse should also produce a trapezoid pulse which is smoother than the original pulse. A comparison of the waveforms of figures 39a and 39b shows that this is indeed the case. The waveform of figure 39b has a much smoother ramp portion, but the rise time of the waveform is essentially the same as that of figure 39a.

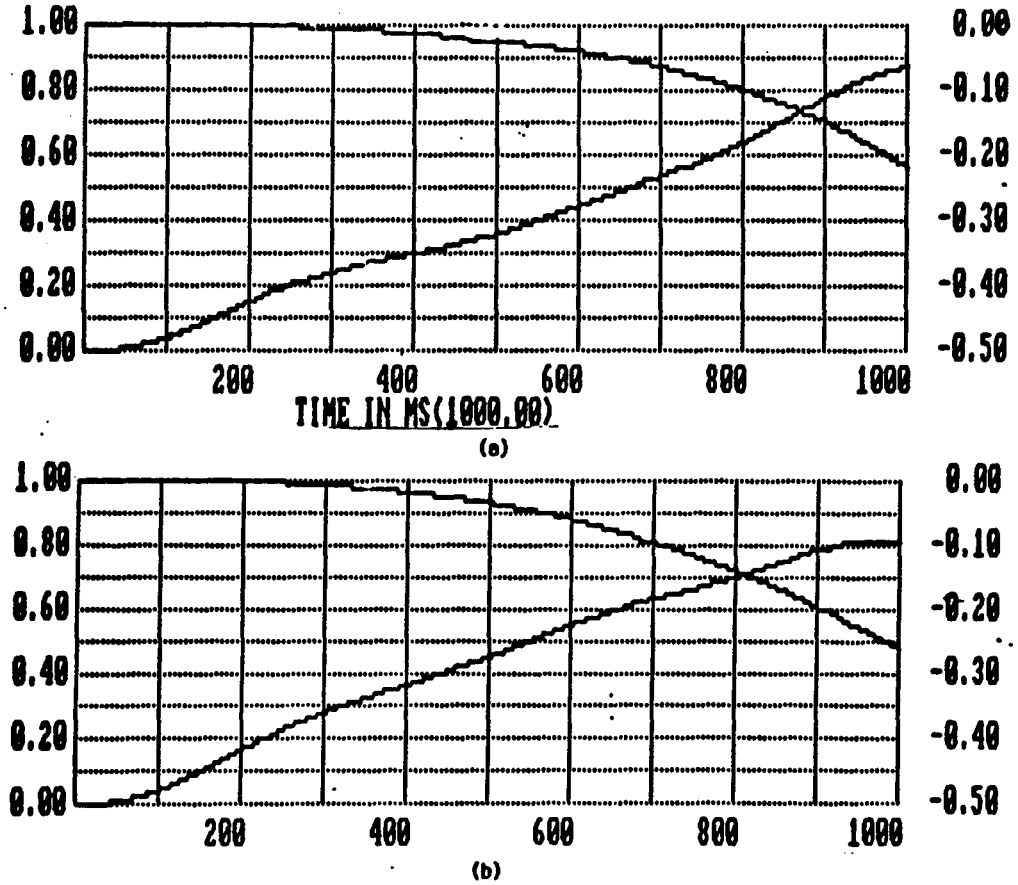

Figure 38- Computer predicted output voltage for the network of figure 23a when (a) C6 is increased by 20%, and (b) C6 is increased by 20% and C2 is decreased by 20%.

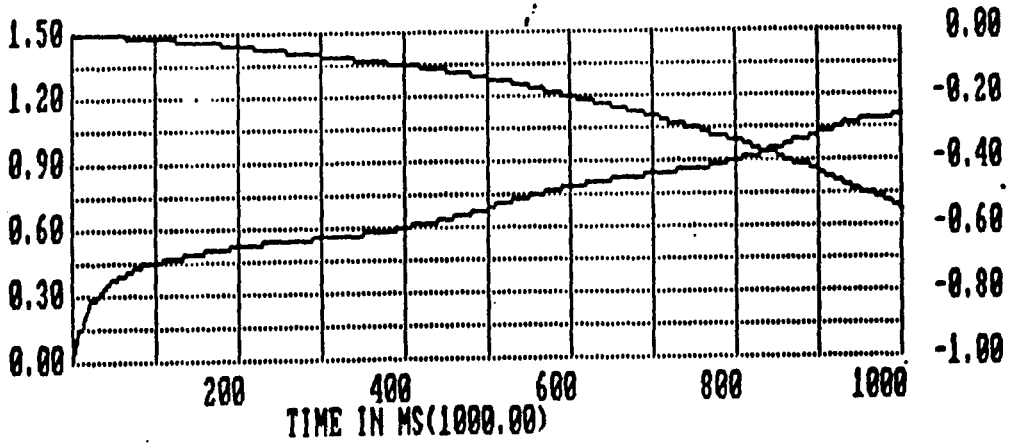

(a)

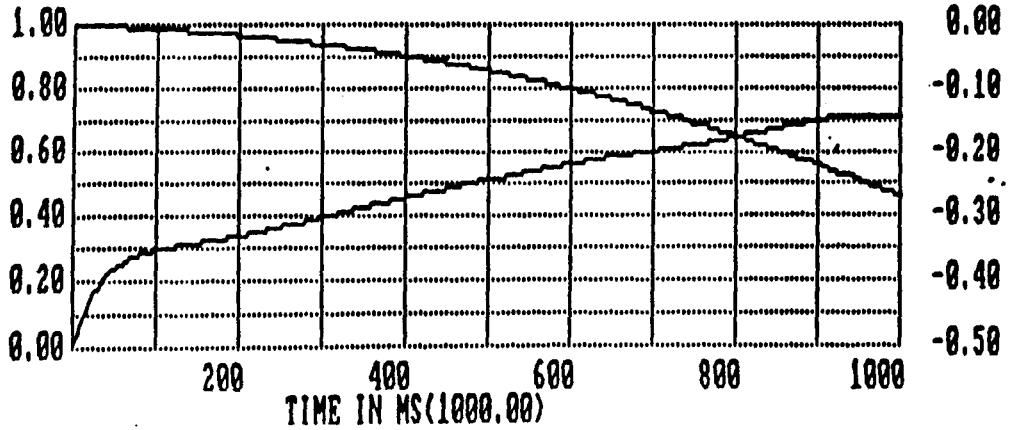

(b)

Figures 39- (a) Computer predicted trapezoid output voltage pulse for the network of figure 23a. (b) Computer predicted output voltage when C6 is increased 20% and C2 is decreased 20%.

The rectangular pulse network sensitivity equations will be the same as those for both the ramp and the trapezoid, with the exception that the even numbered components do not exist, therefore they can not be used to tune the waveform. Even components (C6 and C2) were used to tune each of the waveforms above, so a different approach must be taken in the rectangle case. An attempt was not made to tune the rectangular waveform since networks that produce rectangular waveforms with sharp rise times, no overshoot and maximally flat flattops are well documented. The most complete documentation on this type of network can be obtained by reading chapter 6 of "Pulse Generators" by Glasoe and Lebacqz [4].

Close comparison of the magnitude scales of the sensitivity plots shown in figures 26 through 37 and the actual effect that varying component values has on the output waveform reveals that the magnitude scales are not accurate. The reason for this stems from the initial assumption that was made in order to simplify the sensitivity analysis. The output voltage of the network was assumed to be a simple sum of the individual undamped section currents into a resistive load. This is not the case in reality. The actual output voltage of each section into a resistive load is a damped sinusoidal function. If this is the case the sensitivity equations will take the form of equation 48.

$$S_p^{v(t)} = \frac{K_1 e^{-Kt}\left[\sin\left(\frac{\omega t}{K_2}\right) + \left(\frac{\omega t}{K_2}\right)\cos\left(\frac{\omega t}{K_2}\right)\right]}{i(t)} \qquad (48)$$

In an effort to test this, the actual magnitude changes affected by varying component values were plotted for several inductors and capacitors in the

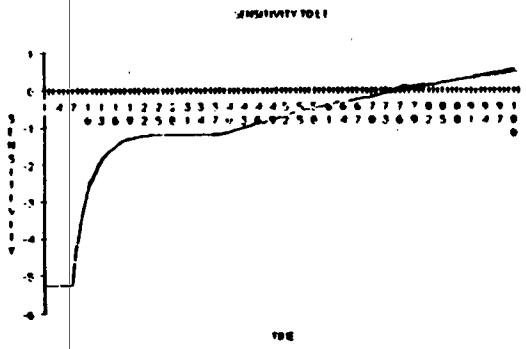

(40)

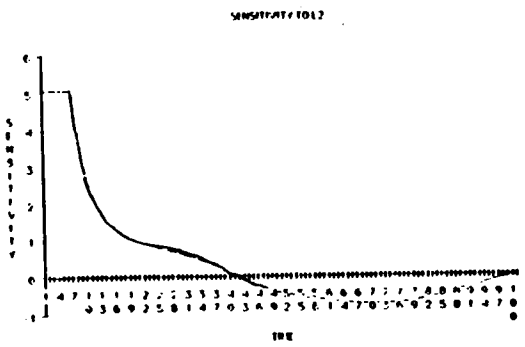

(41)

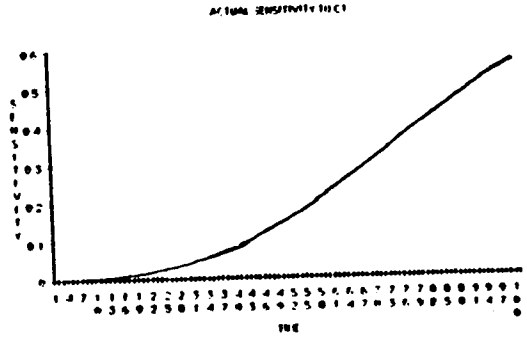

(42)

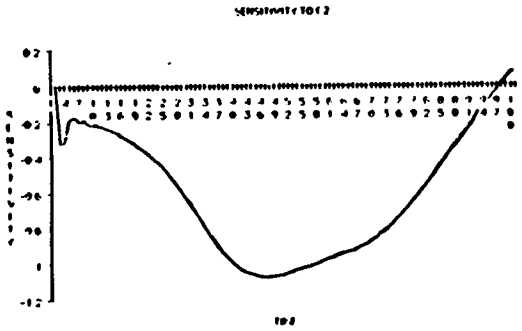

(43)

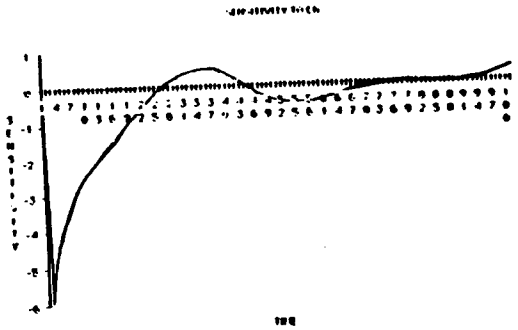

(44)

Figures 40 through 44- Actual sensitivities of the output voltage of the network of figure 23a to component variations. Note: The flat portion near t=0 in figures 40 and 41 is a result of the removal of several data points near the beginning of the plot. This was done in order to allow the spreadsheet program to plot the remaining data on a legible scale.

network. These plots are shown in figures 40 through 44. In order to obtain these plots the component in question was increased by 10%. A spreadsheet program was then used to calculate the relative deviation of the output voltage 10 milliseconds of the nominal 1 second output. Figures 40 through 44 are the plots of these relative deviations. Comparison with the appropriate plots in figures 26 through 37 shows that the actual deviation plots have the same oscillatory behavior, but the magnitude of the oscillations is different and tend to decrease with increasing time. This means that the sensitivity plots of figures 26 through 37 are at least qualitative in that they tell you which parts of the waveform are affected by each component. In a tuning mode this type of information is all that is needed since the person that is doing the tuning will just guess what component needs to be varied and then just keep adjusting the value of the component until the desired results are achieved. The actual sensitivity plots also suggest that the sensitivity of the output voltage waveform to component variations is usually less than 1, especially for the higher numbered sections. This means that component tolerances used to specify the components of which the network is constructed can be relaxed accordingly. This will result in a significant decrease in the cost of each pulser circuit. The discovery that the same optimized network can be used to produce both trapezoid and ramp pulses will also result in a per unit cost decrease for the pulsers, since all networks will be same and quantity discounts will be available for components used to fabricate the networks. Testing costs will also decrease since a single prototype pulser can be used to investigate the viability of all trapezoid and ramp pulser circuits.

7.0 BENCH TEST RESULTS

In order to get an idea as to whether the networks that were derived and modelled above would actually perform as expected, a test network was built. Due to limitations on time, cost and available components it was decided to fabricate a network that would produce pulses with durations near 1 microsecond, like those required for ILSE, but with peak amplitudes of only several tens of volts instead of several tens of thousands. If a network of this type performed as predicted, fabricating a network capable of larger peak amplitudes should be possible by only increasing the power handling capability of the individual components.

The most difficult component to obtain was the inductor, therefore, an available value of inductance was chosen and the rest of the network was designed around it. In this case the size of the inductors that were readily available was 50 micro-henries. If a pulse approximately 1 microsecond in duration is desired the impedance scale factor for the network of figure 13 will be 100. The time and impedance scaled network used for the bench tests is shown in figure 45a. The computer predicted output for the network is shown in figure 45b.

In the first network that was fabricated for the bench tests SCR's were used as the output switches. Capacitance values in the actual network also varied from the nominal values needed to represent the network of figure 45a exactly. These initial tests were also conducted with a load resistance of 92 ohms instead of the "matched" load resistance of 275 ohms. The reason being that the matching

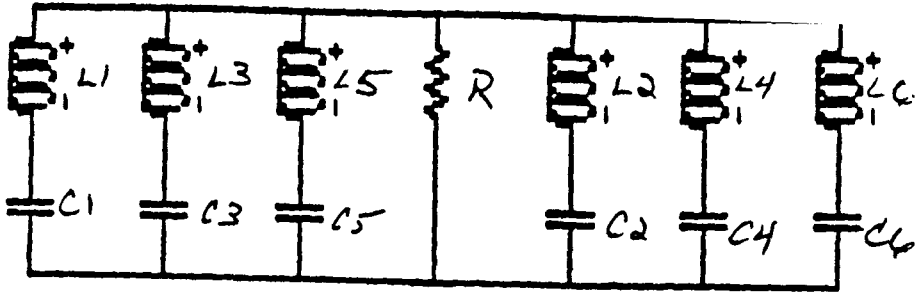

L1=L2=L3=L4=L5=L6= 50 micro-henries

C1= 2030 pf C2= 507.5 pf

C3= 225.6 pf C4= 126.9 pf

C5= 81.2 pf C6= 56.4 pf

(a)

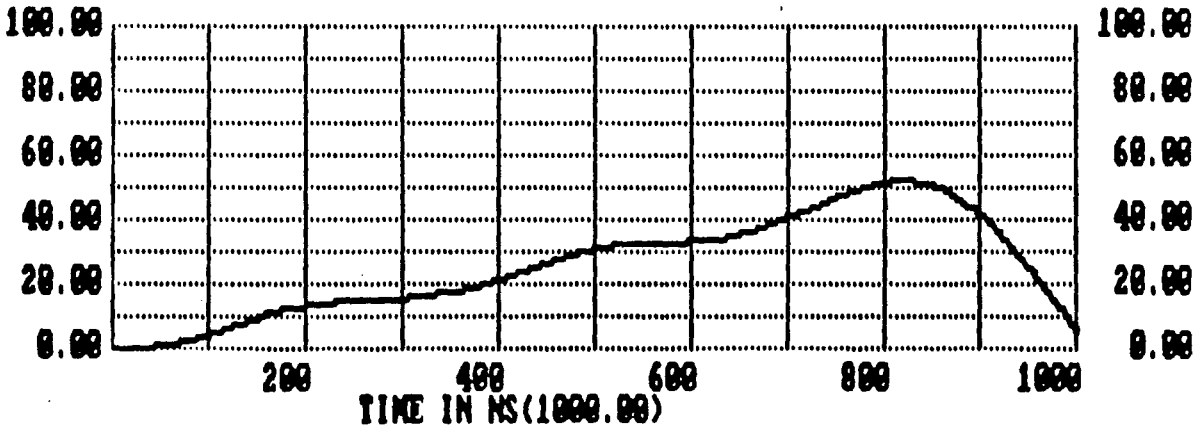

(b)

Figure 45- (a) Theoretical time and impedance scaled network used for bench tests. (b) Computer predicted output waveform for a load resistance of 92 ohms and vcn(0-)= +/- 100 volts for the odd and even sections, respectively.

resistance analysis had not yet been completed and a load resistance of 1 ohm was assumed for the network of figure 13. The actual network used to test theperformance of the bi- polar PFN concept is shown in figure 46 and the predicted output for various initial voltages are shown in figures 47a and 47b. Oscilloscope plots of the actual voltage waveforms for various initial voltages are shown in figure 48. As can be seen by comparison of the appropriate figures the actual oscilloscope closely resemble the plots predicted by the computer simulation. The most notable differences being:

1. The peak magnitudes of the actual plots are slightly lower than those predicted by the computer.
2. There is a large "bump" in the waveform at approximately 550 nanoseconds.

The peak magnitude differences can be attributed to lossy components such as inductors and switches and does not present a real problem since it can be compensated for by simply increasing the initial voltages on the network. The bump is a different story since it represents an unsatisfactory perturbation in the waveform and its elimination is addressed in the following section.

7.1 Eliminating the "bump"

The bump observed in the waveform is not predicted by the computer simulations and finding the cause of the bump and eliminating it may at first seem like trying to find a needle in a haystack. This is the case until the question is asked: "What is in the actual circuit that is not accounted for in the computer model?". The answer is, the two SCR switches used to discharge the network sections into the load. To account for these switches diodes were added to the

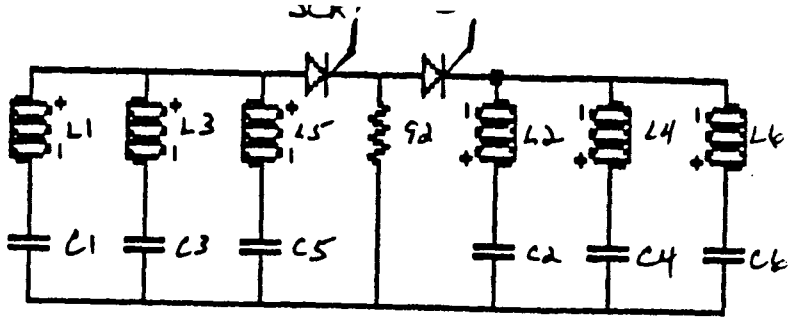

L1=L2=L3=L4=L5=L6= 50 micro-henries

C1= 2000 pf C2= 510 pf

C3= 220 pf C4= 130 pf

C5= 82 pf C6= 55 pf

Figure 46- Actual network used for bench tests.

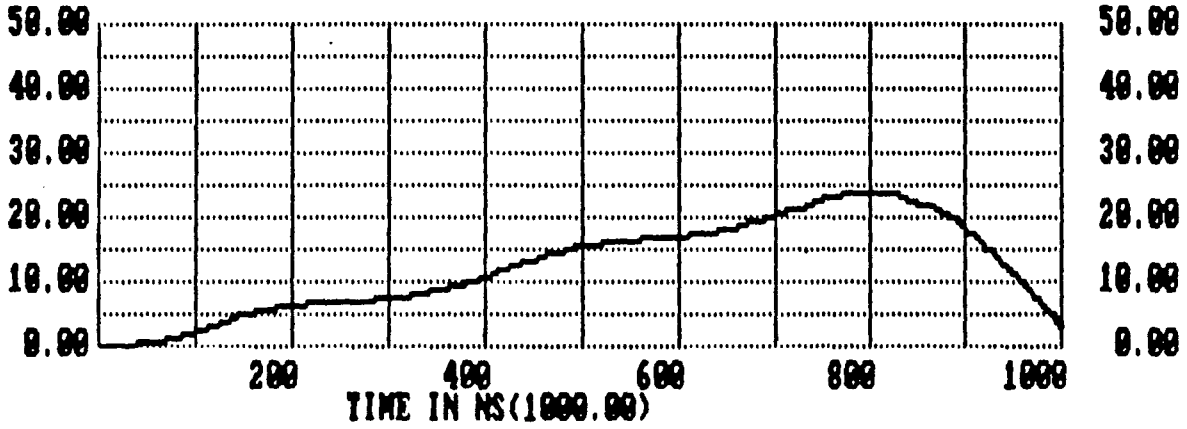

(a)

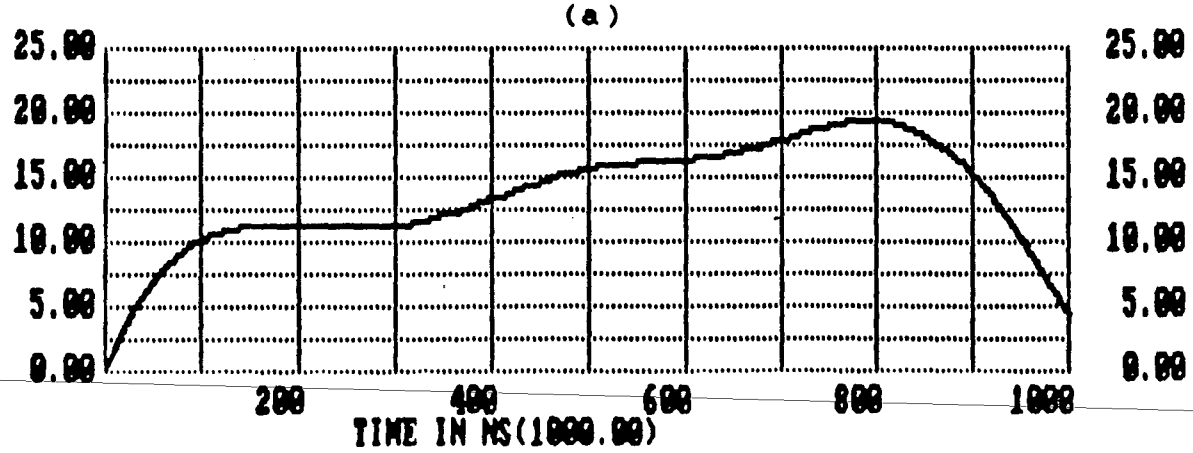

(b)

Figure 47- Computer predicted output voltage waveforms of network of figure 46 for (a) $v_{c1}(0-)$= +/-50 volts, odd and even sections, respectively, and (b) $v_{c1}(0-)$= +50 and -16.67 volts, odd and even sections, respectively.

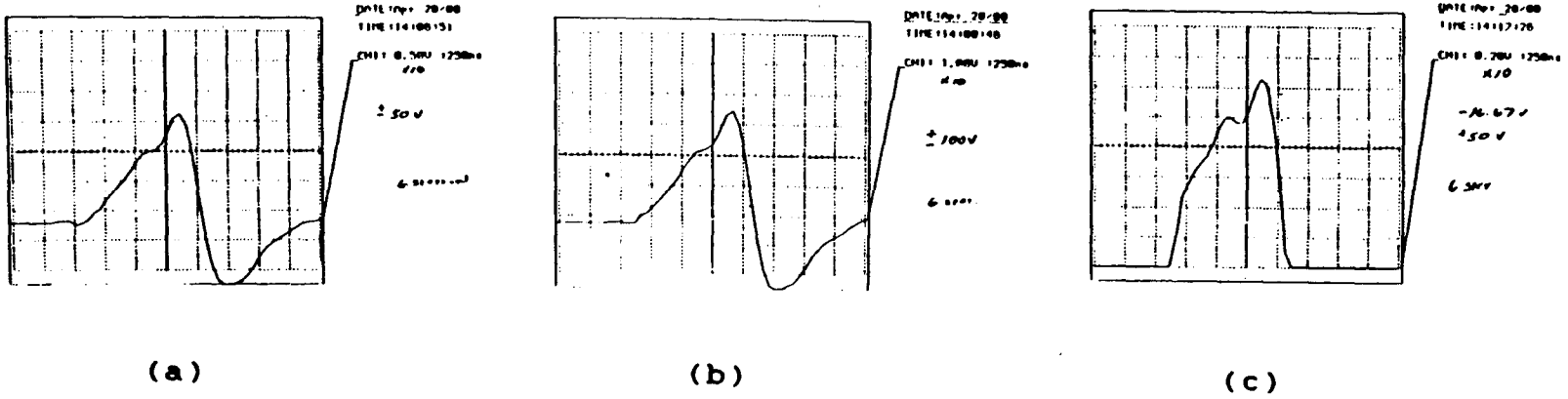

(a) (b) (c)

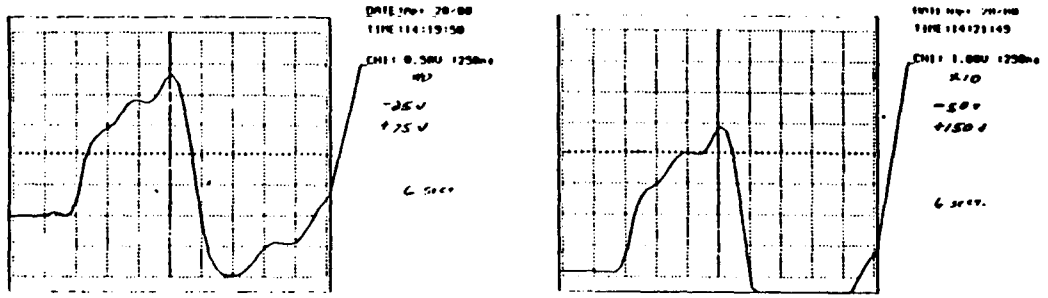

(d) (e)

Figure 48- Actual oscilloscope plots of output voltage of the network of figure 46 for various initial capacitor voltages.

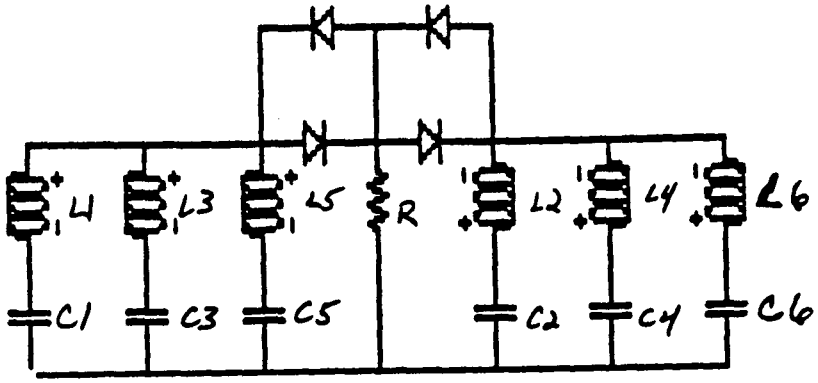

Figure 49- Computer model of the network of figure 46 with diodes added.

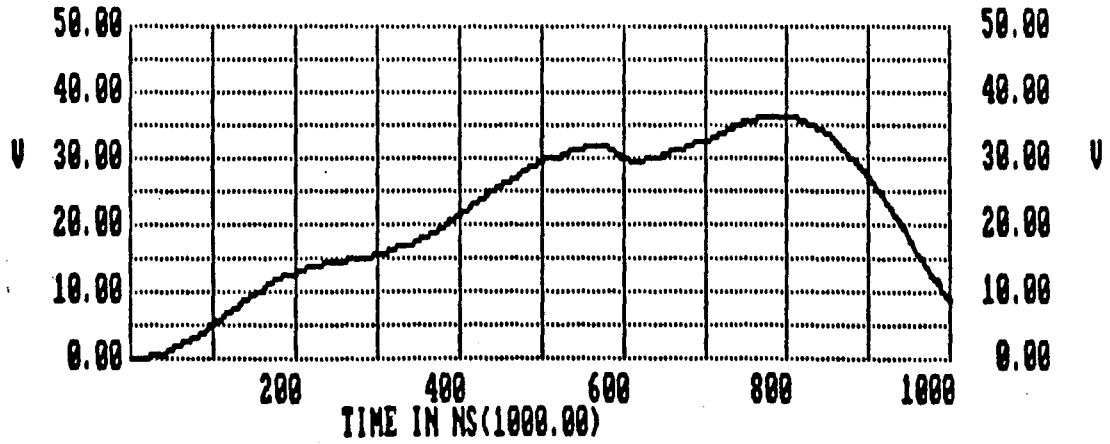

Figure 50- Computer predicted output voltage waveform for the network of figure 49.

computer model as shown in figure 49. Diodes also have some series resistance and a limited di/dt when they first begin to conduct. To account for the limited di/dt a small amount of series inductance was also added to the model. Figure 50 is the computer predicted load voltage waveform when these items are added to the model. Note that there is a bump in the waveform at approximately the same time as that observed in the actual circuit. Figure 51 is a plot of the predicted output voltage and the voltage across the diodes that connect the even harmonic sections to the load. Note that the bump in the waveform occurs when these diodes are switching, i.e. one is being reverse biased and the other is being forward biased. The bump must be caused by the finite switching times and limited di/dt of the diode switches used to fabricate the circuit.

Field-Effect-Transistors (FET's) were then used in place of the SCR switches used in the original tests. FET's were chosen because they have extremely low turn-on times (< 10 nanoseconds) and high di/dt's. The load resistance was also increased to 282 ohms, much closer to matched load resistance for the network. Figures 52a and 52b show the actual output voltage waveforms for two different sets of initial voltages. Note that the amplitude of the bump has been decreased.

7.2 Bench Test Tuning Results

The sensitivity analysis showed that the sensitivity plots shown in figures 26 through 37 can be used to optimize or "tune" output waveform. This was attempted during the bench tests. Figures 53a and 53b show the actual output voltage of the network when the value is increased to 67 pf and 76 pf, respectively. Note that the ripple in the waveforms has been reduced. An attempt

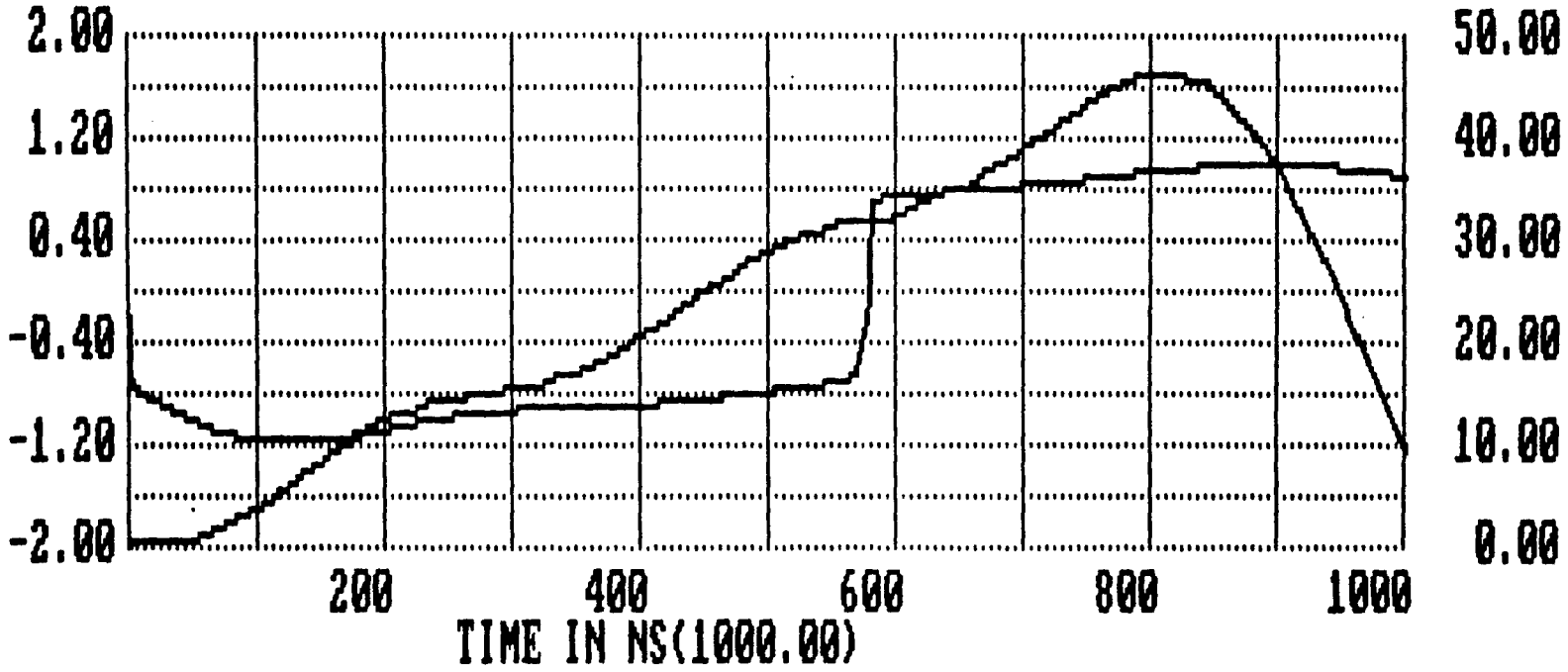

Figure 51- Computer predicted output voltage of the network of figure 49 with the even harmonic diode voltage superimposed. Note that the diodes are switching at the time the bump occurs.

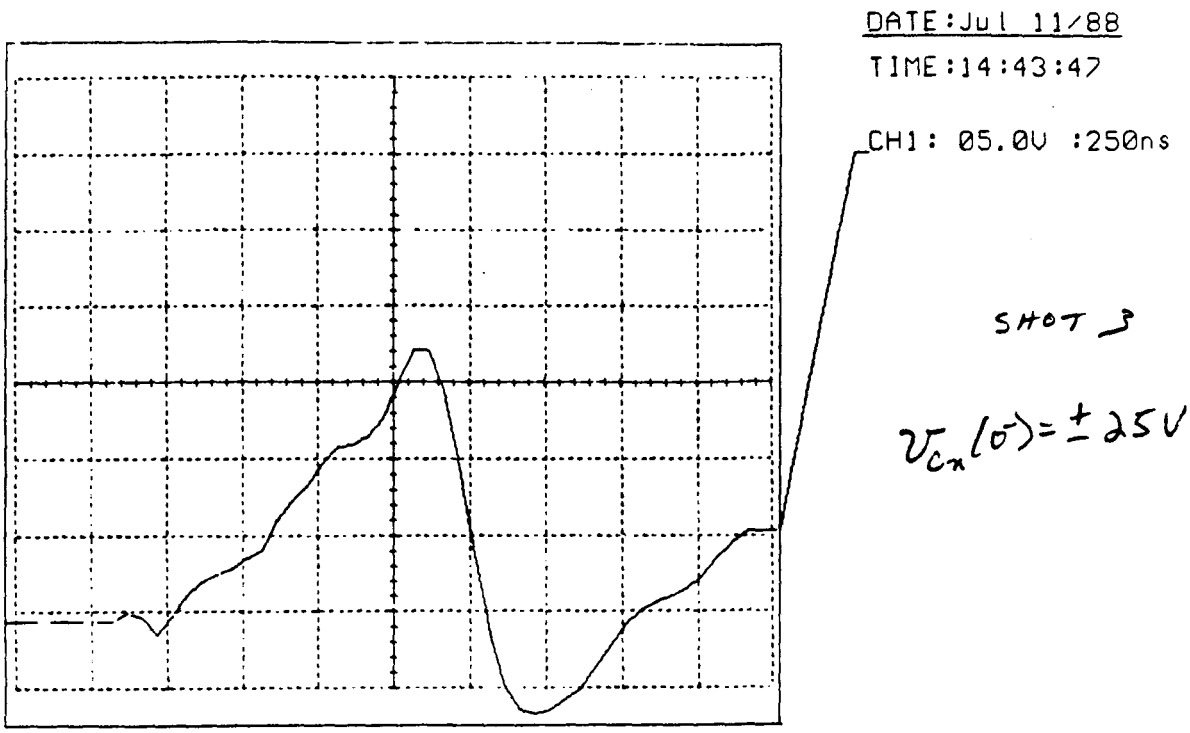

(a)

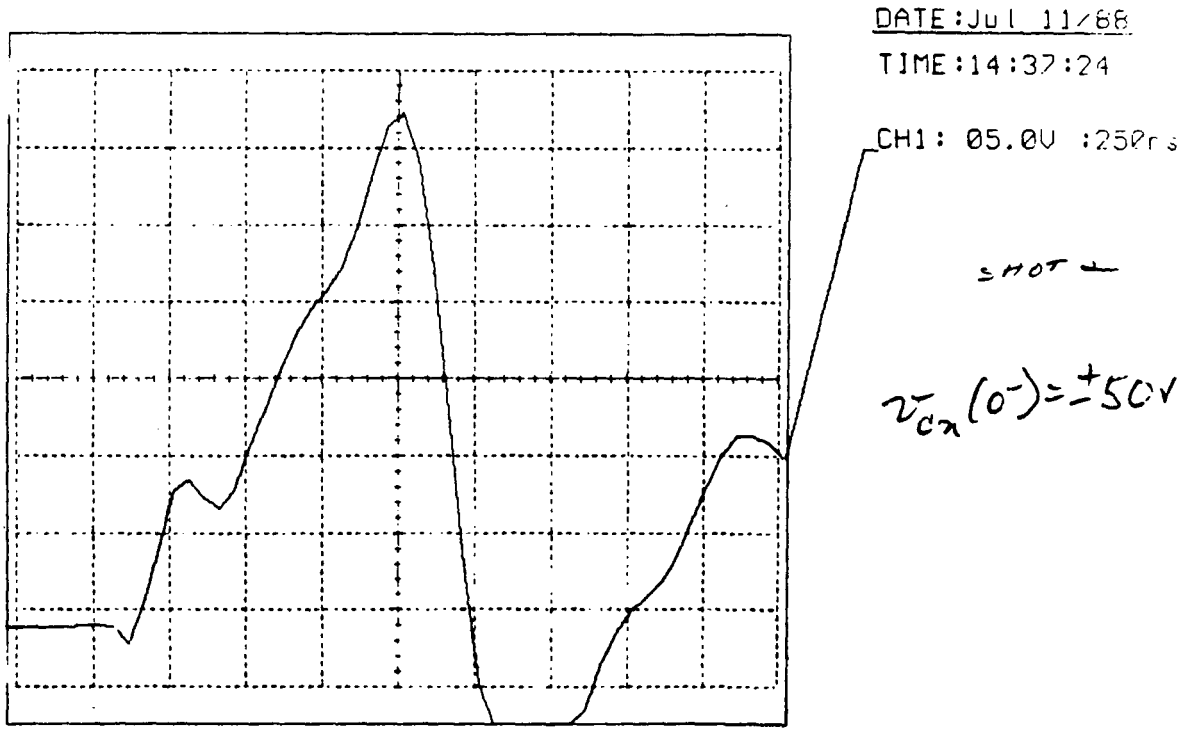

(b)

Figure 52- Actual oscilloscope plots of the output voltage of the network of figure 46 with the SCR switches replaced by FET's.

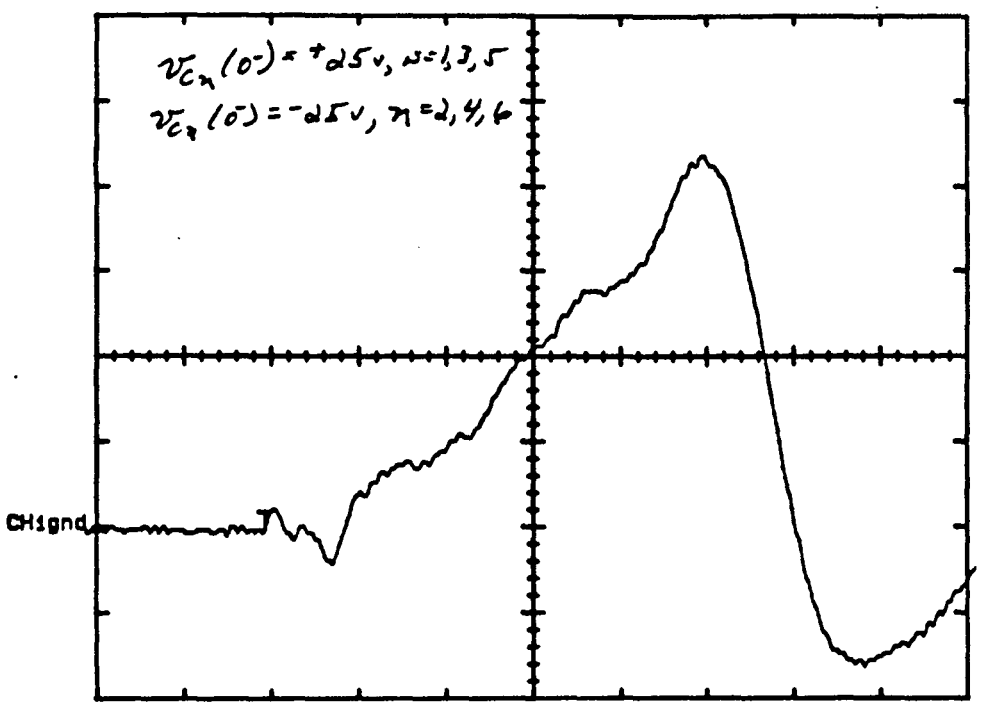

(a)

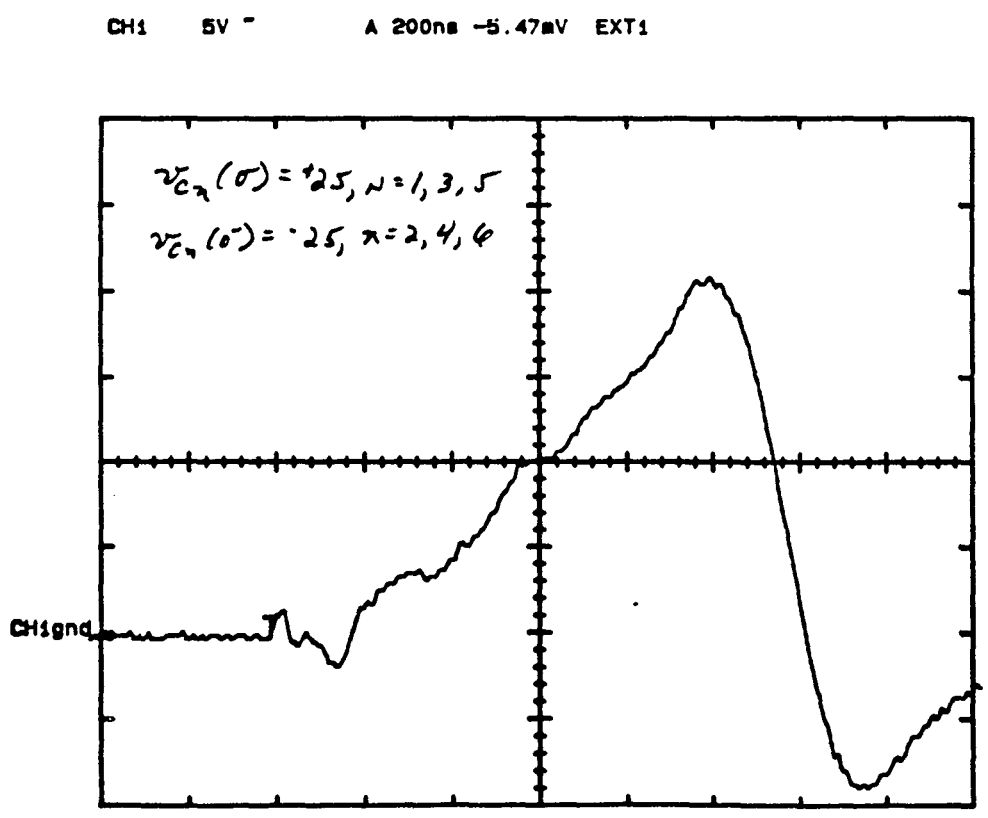

(b)

Figure 53- Actual oscilloscope plot of the network output voltage when C6 is increased to (a) 67 pf, and (b) 76 pf.

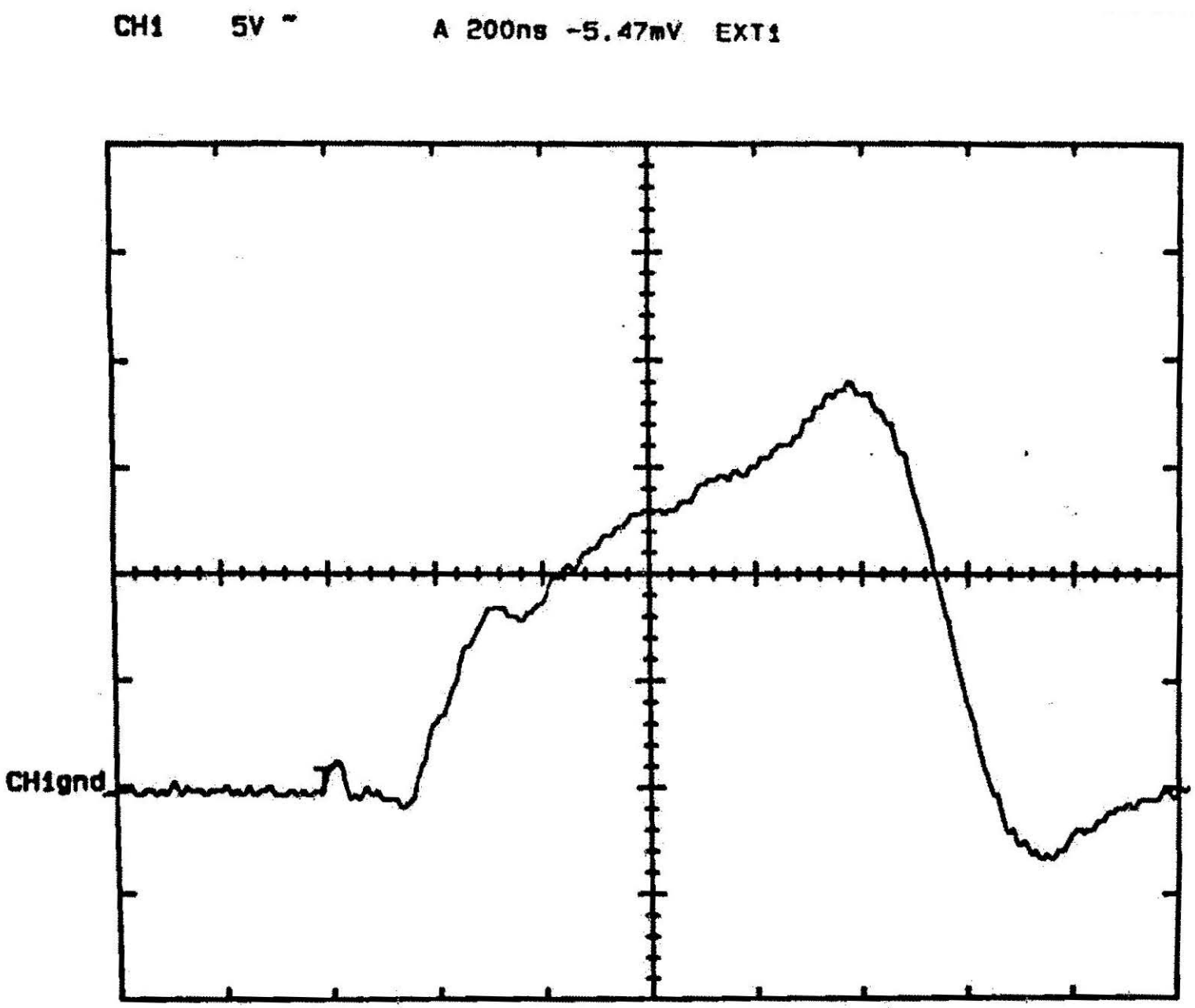

Figure 54- Actual oscilloscope plot of network output voltage when vcn(0-)= +25 volts and -8.33 volts, odd and even sections respectively.

was also made to increase C2 as was done in the computer tuning phase above, but it proved to be unsuccessful. This is possibly due to the fact that capacitors with tolerances of +/-10% were used, meaning that C2 may have already been greater than the nominal value. Figure 54 is the actual output waveform for same network with initial voltages of +25 volts (odd harmonic sections) and - 8.33 volts (even harmonic sections). Note that the same smoothing effect is observed.

7.3 Bench Test Conclusions and Observations

1. The bump observed in the initial circuits that used SCR switches shows that great care must be taken when selecting the actual output switches for the PFN. The switch must be "fast", i.e. several nano-second turn on times, and the switch must be capable of conduction in both directions once closed and also have low on resistance and inductance once it is turned on.
2. Tuning using the sensitivity plots as a guide should be done both on the computer and on an actual circuit. This will help to eliminate the problems caused by non-ideal components.
3. As can be seen by the actual waveforms shown in figures 55a and 55b, the network does approximate a continuous function, not a transient pulse.
4. All components used in the fabrication of the test circuit had tolerances of +/- 10%. The fact that the actual circuit performance was close to the predicted performance reinforces the conclusion stated above that the sensitivity of the output waveform to any component variation in less than one.

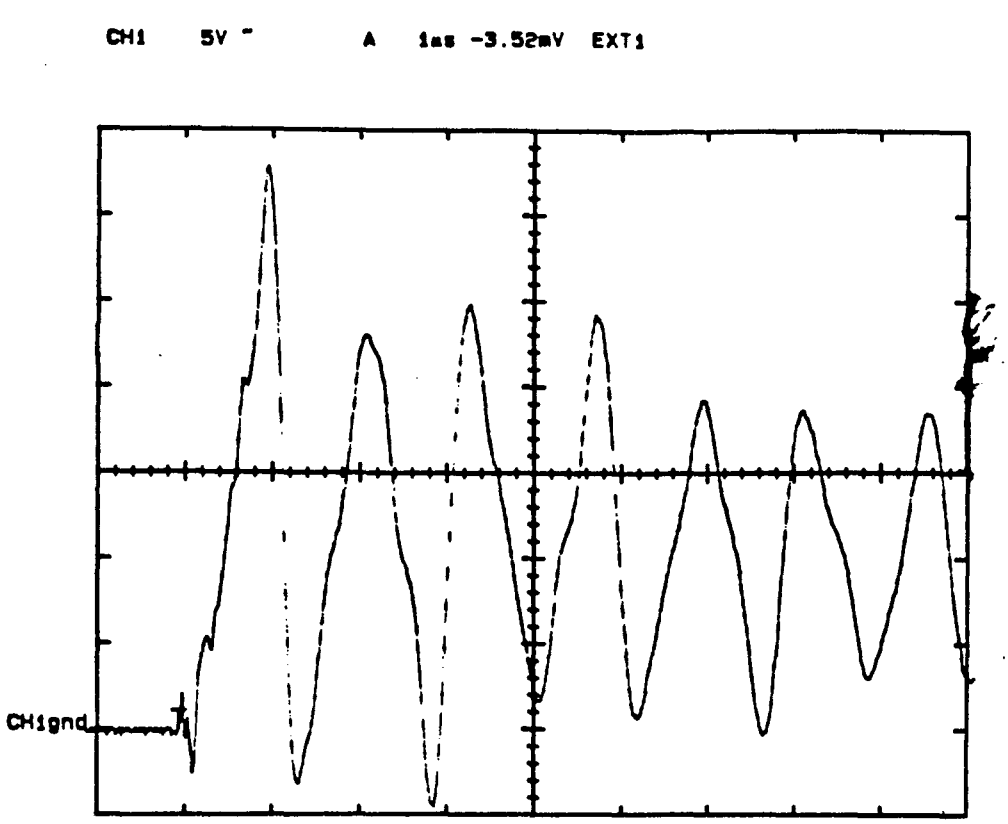

(a)

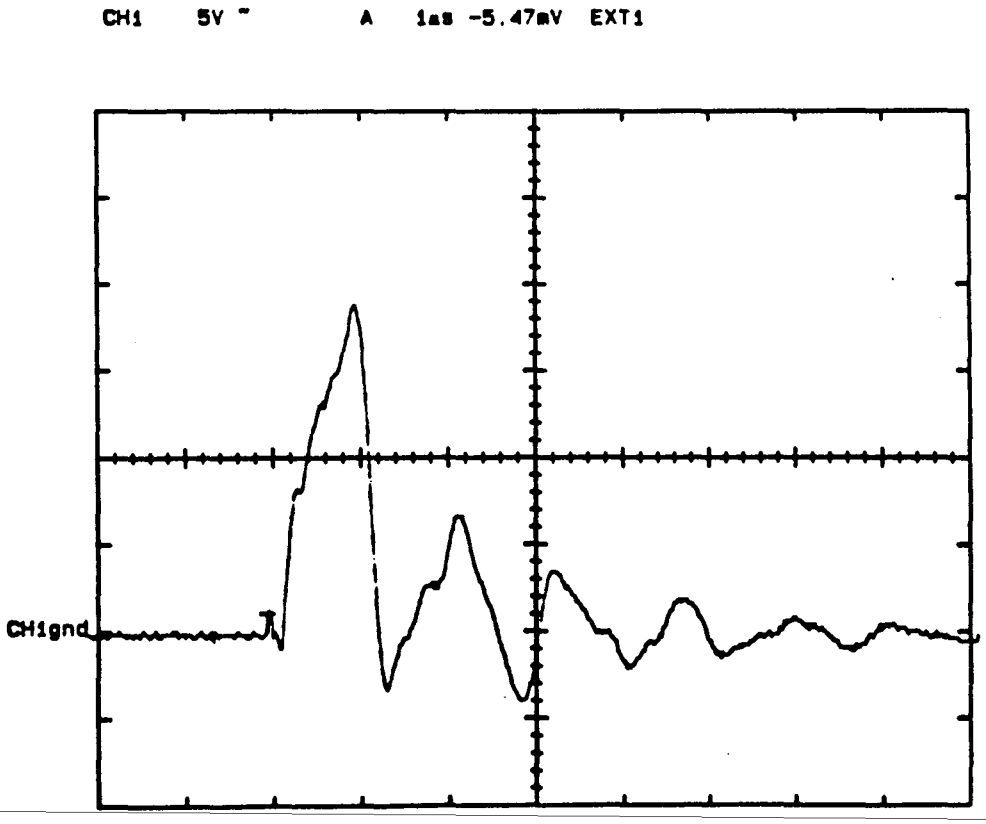

(b)

Figure 55- Actual oscilloscope plots of network output voltage showing that the network does indeed approximate a continuous function as opposed to a transient pulse.

8.0 PULSE-FORMING-NETWORKS FOR ILSE

The impedance presented to the network by the actual cores to be used for the magnetic acceleration portion of ILSE is mostly resistive, but there is a slight inductive component. The actual equivalent circuit for the load is a resistor in parallel with an inductor. The equivalent circuit for one four inch ILSE core is shown in figure 56. The values for the circuit were determined from conversations with LBL personnel familiar with METGLAS cores [9].

At the time this study was being conducted the actual duration of the pulses required for ILSE had not been determined exactly, so a nominal duration of 1 microsecond has been assumed. This assumption is valid since any network developed for a 1 microsecond pulse can be time scaled to the proper duration. Also, pulses that are slightly longer than required are not a problem since it is not important what the core voltage pulse does once the ion-beam has passed.

In order to reduce the amount of hardware required the three cores in each gap should be driven by one PFN. If the cores are connected in parallel the magnitude of the pulse needed from the PFN is just one third of the required gap voltage. The equivalent circuit for three parallel cores is shown in figure 57. In order to obtain the values for the PFN needed to drive this load the normalized network of figure 23a must be time and impedance scaled. The time scaling of the network is obvious, but then what is the impedance scale factor for the equivalent circuit of figure 57? The simplest choice is to scale the network to match the 13.3 ohm resistive component. This leads to the network of

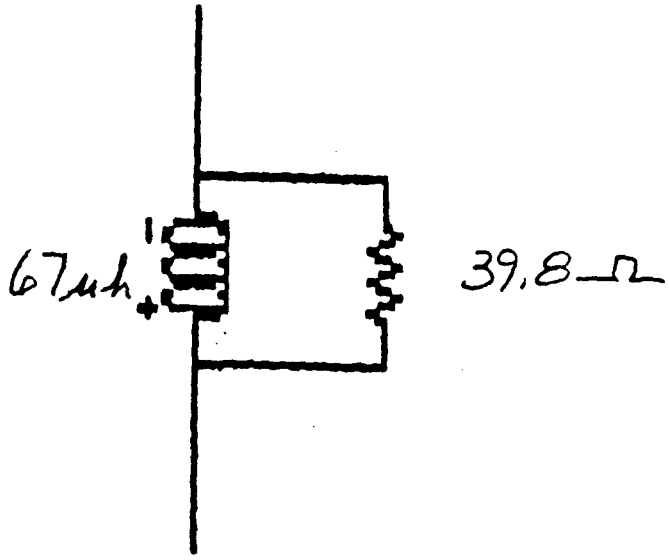

Figure 56- Equivalent circuit for one 4 inch ILSE core. [9]

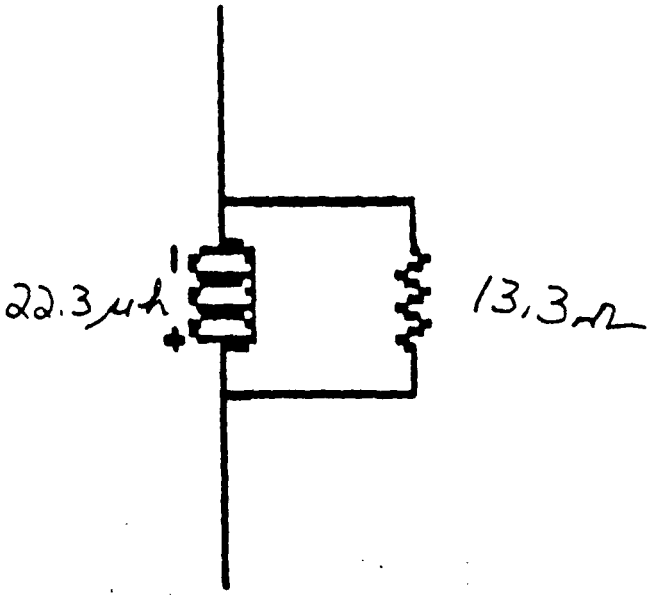

Figure 57- Equivalent circuit for three 4 inch ILSE cores connected in parallel.

figure 58a. The computer predicted output waveform is shown in figure 58b. Notice that the voltage transfer efficiency is not quite as high as the efficiency for a matched resistive load. This is due to the impedance effects of the parallel inductance.

The sensitivity analysis of the network and the fourier series representation of the waveform tell us that the first harmonic has the most affect on the output waveform. The first harmonic in this case is 500 KHz. The impedance of the inductor at 500 KHz is approximately 70 ohms. The equivalent impedance of 13.3 ohms in parallel with 70 ohms is 11.2 ohms. The network of figure 59a is matched to 11.2 ohms. The predicted output waveform is shown in figure 59b. Notice that the voltage transfer efficiency has been increased. If higher voltage transfer efficiencies are desired the network impedance can be reduced, but it should be noted that voltage efficiency comes at the expense of energy efficiency (refer to figures 18, 22, and 25).

The sensitivity analysis also showed that the network can be tuned to produce smoother ramp pulses. The network of figure 59a has not been optimized for smooth ramps and trapezoids. The reason for this is that the bench tests showed that the actual network output is slightly different from that predicted by the computer simulations. The differences are due to such things as stray capacitance and inductance not accounted for in the computer model. The most effective means of tuning for the optimum output pulse is to build a full size prototype network and tune experimentally using the sensitivity plots of figures 26 through 37 as a guide. The optimum experimental network component values can then

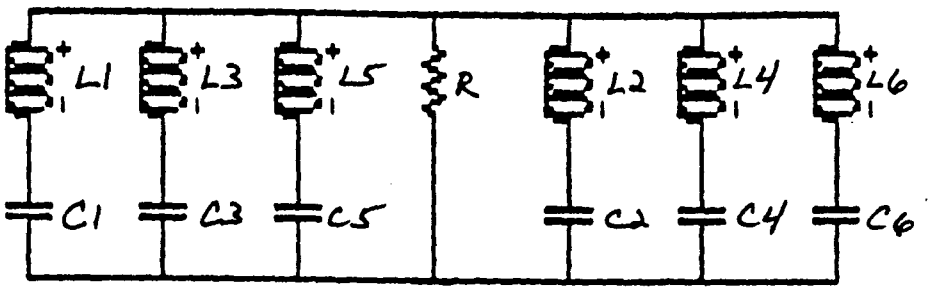

L1=L2=L3=L4=L5=L6= 3.019 micro-henries

C1= 52.53 nf C2= 13.13 nf

C3= 5.836 nf C4= 3.283 nf

C5= 2.101 nf C6= 1.459 nf

(a)

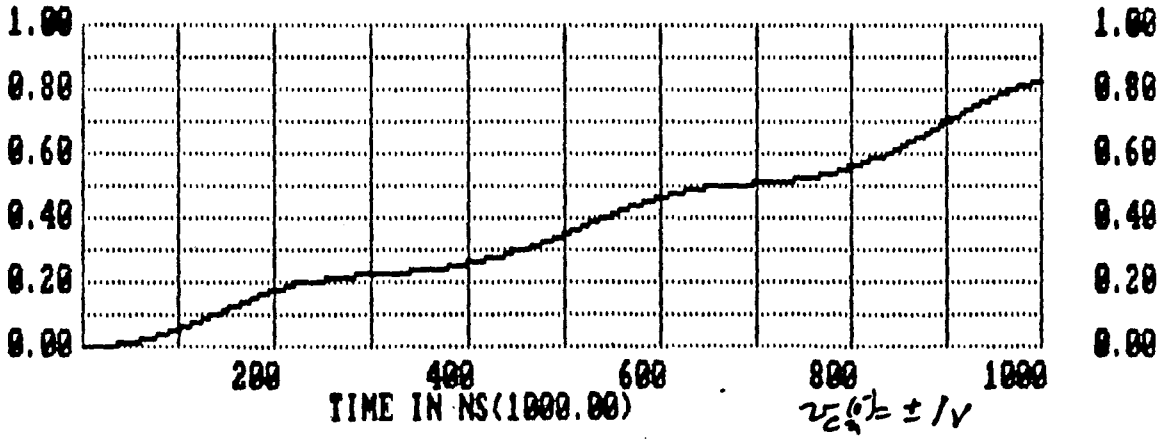

(b)

Figure 58- (a) Bi-polar, one micro-second, 13.3 ohm PFN. (b) Computer predicted output voltage waveform into the equivalent circuit of figure 57.

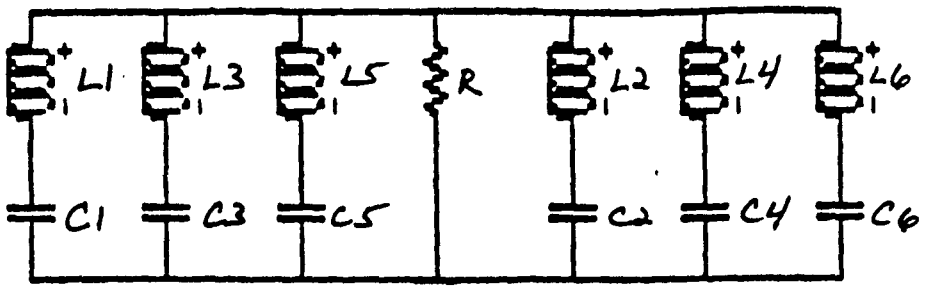

L1=L2=L3=L4=L5=L6= 2.542 micro-henries

C1= 62.38 nf C2= 15.59 nf

C3= 6.931 nf C4= 3.898 nf

C5= 2.495 nf C6= 1.733 nf

(a)

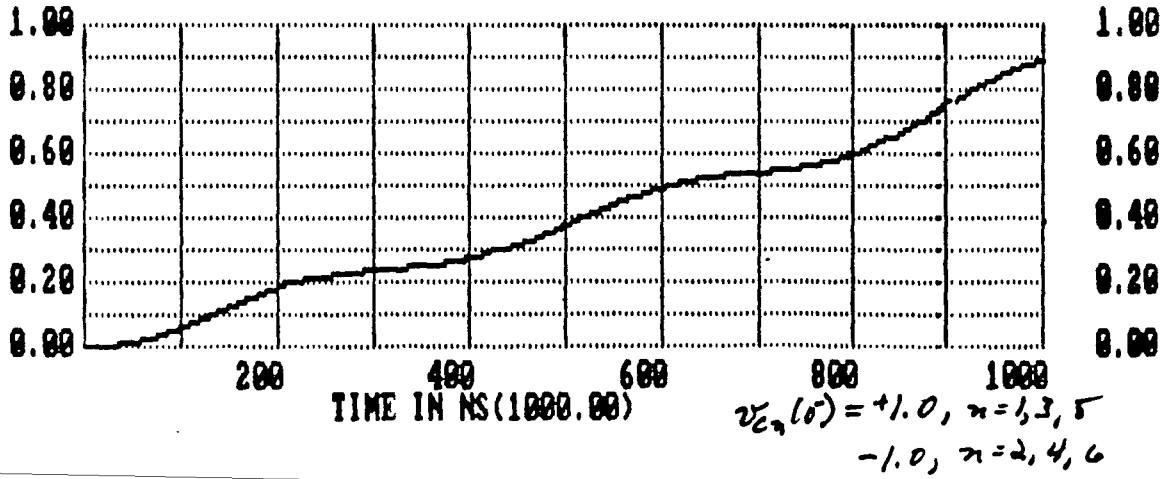

(b)

Figure 59- (a) Bi-polar, one micro-second, 11.2 ohm PFN. (b) Computer predicted output voltage waveform into the equivalent circuit of figure 57.

be used to fabricate the networks needed for ILSE. Time and budgetary constraints did not allow this to be included in the scope of this study, but estimated costs for such a prototype network are included in the cost section of this report. Using this technique it should be possible to find a network capable of approximating ramp and trapezoid pulses to within several percent.

The specifications for the ILSE pulsers call for magnitude variations of less than one percent. While it may be possible, it is not probable that a bi-polar PFN can meet this specification, therefore, correction cores will be necessary in the final ILSE configuration. The increased complexity introduced by adding these correction cores will need to be weighed against the inherent simplicity of the bi-polar PFN concept.

The ILSE specifications also call for pulse to pulse variations and trigger delay jitter of less than one percent and 20 nano-seconds, respectively. The trigger delay jitter is only dependent on the jitter of the switch and switch trigger circuits used. Twenty nano-seconds is well within the range of commercially available spark gaps and spark gap trigger circuit. The pulse to pulse variations of a bi-polar PFN are dependent on the variation of component values and are a function of initial network voltage variations. The sensitivity analysis showed that the sensitivity of the output pulse to component variations is less than 1, therefore pulse to pulse component variations of one or two percent should be used as a specification in the fabrication of actual pulser components. The sensitivity of the output waveform to initial voltage variations is one, therefore, the charging supplies used in the network should have a voltage regulation

specification of much less than one percent. This should present no real problem since commercially available high voltage power supplies often have regulation specifications of 0.1%.

9.0 PULSER COST AND SCHEDULE

The following is the Work Breakdown Structure (WBS) under which the construction and testing of a full size prototype pulser required to test the feasibility of using bi-polar PFN's for the pulsers in the magnetic acceleration portion of ILSE. Costs are listed on a per pulser basis.

1.0 Magnetic Acceleration

- 1.1 Capacitors- Capacitors will be procured from a manufacturer. In order to decrease costs as much as possible the capacitance values required to fabricate the sections will be constructed by piecing together off-the-shelf capacitors. Sensitivity analyses and bench tests indicate that the capacitor tolerances need not be better than +/- 5%. Some small trim capacitors may be needed to bring bulk capacitances into tolerance. 120 days should be allowed for delivery.
- 1.2 Inductors- Inductors will be procured from a manufacturer. Sensitivity analyses and bench tests indicate that the inductor tolerances need not be better than +/- 5%. 120 days should be allowed for delivery.
- 1.3 Switches- Off-the-shelf spark gap switches will be procured. Trigger circuits will be designed and fabricated. 1.5 manweeks have been costed for design and fabrication of the trigger circuits.

1.4 Charging Supplies- Charging supplies for the even and odd harmonic sections and the spark gap trigger circuits will be procured from a manufacturer.

1.5 Cabling and Assemblies- Inductors and capacitors will be connected together to form sections and sections will be packaged together to form a network. The Network will be installed and output cabling connected. 5 manweeks have been costed for assembly and connection of the pulser.

1.6 Control and Monitoring- Simple switch trigger circuits, load voltage and current monitors, and charging voltage monitors will be designed, fabricated and installed. 7.5 manweeks have been costed for the design and fabrication of the control and monitoring circuits.

Costs for 1.0

WBS	Manpower	Equip
1.1 Capacitors	0	$ 6.0K
1.2 Inductors	0	$ 4.0K
1.3 Switches	$3.0K	$ 7.0K
1.4 Charging supplies	0	$ 8.0K
1.5 Cabling and assemblies	$10.0K	$15.0K
1.6 Control and monitoring	15.0K	$ 5.0K
Subtotal	$28.0K	$45.0K
Total		$73.0K

10.0 CONCLUSIONS AND RECOMMENDATIONS

1. The bi-polar PFN concept developed during this project can be used to design networks that will approximate non-rectangular pulses. In this case the pulses were ramps and trapezoids. The normalized one ohm, one second network is shown in figure 60. The equation for the initial network voltages is also shown in

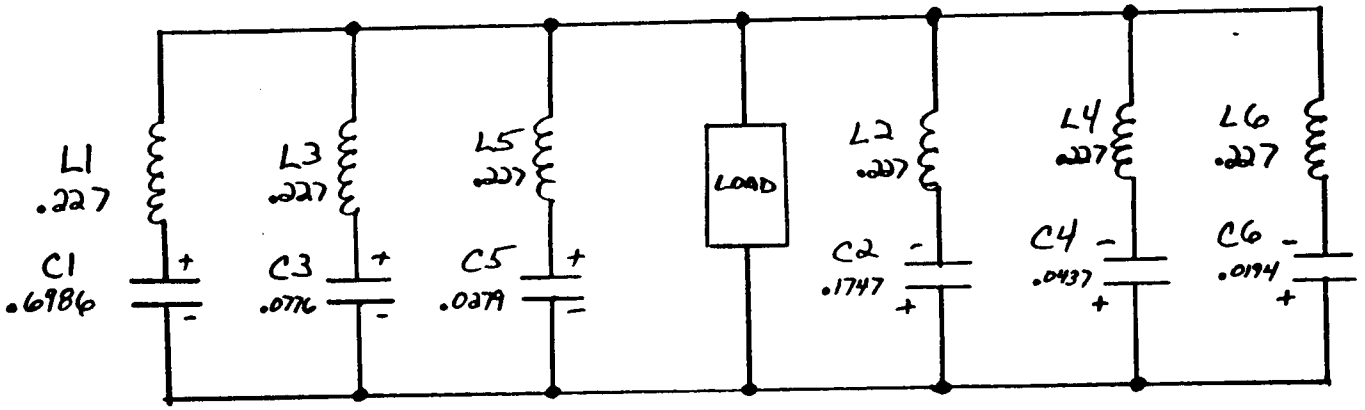

$$V_{CN}(0-) = [(-1)^{N+1} + x]KTR$$

where x=0 for a ramp

x<1 for a trapezoid

Figure 60- Normalized, one ohm, one second, bi-polar Pulse Forming Network

figure 60. This network can be impedance and time scaled to produce pulses of different durations into different load resistances.

2. The voltage transfer efficiency of the bi-polar PFN can be increased at the expense of energy transfer efficiency.

3. The sensitivity plots of figures 26 through 37 can be used as a guide when tuning the output pulse of the PFN. Networks that have been tuned will produce smoother ramps and trapezoids while still maintaining sharp rise time characteristics.

4. The network shown in figure 60 is a type C PFN. This network can be transformed into other Guillemin type networks using Cauer and Foster transformations [7]. The major advantage that the type C network offers is that each section of the network produces one harmonic of the fourier series. In other network types all sections contribute to all harmonics. The major disadvantage of the type C is that all capacitors must be able to handle full voltage reversal. These types of capacitors tend to have shorter lifetimes and higher per unit costs [10].

5. The sensitivity plots of figures 26 through 37 are only qualitative in nature. The actual sensitivity plots for component variations are damped sinusoids with magnitude peaks much less than one, therefore standard off-the-shelf components with tolerances of +/- 10% can be used for most applications.

6. Great care must be taken when selecting output switches for the network. Switches must be able to conduct both ways once triggered and they must have internal inductances much lower in value than the inductors used in the network.

7. A much larger bi-polar PFN should be built. The actual performance of this network should be measured and quantitatively compared to the desired ramp and

trapezoid pulse shapes. This study was more qualitative in nature and the purpose of the study was to investigate if the bi-polar PFN concept would work at all.

REFERENCES

1. T. Fessenden, "A Straw Physics Design For ILSE", Presentation made to HIFAR Group a Lawrence Berkeley Laboratory, January 14, 1988.
2. A. Faltens, S. Rosenblum, C. Smith, "Investigation of Metglas Toroid Fabrication Techniques for a Heavy-Ion Fusion Driver", Journal of Applied Physics, April 15, 1985.
3. D.E. Gough, D.A. Brodzik, "Pulser Development for MBE4", IEEE Transactions for 17th Modulator Symposium, June 1986.
4. G.N. Glasoe, J.V. Lebacqz, "Pulse Generators", Dover Publications Inc., 1948.
5. W.E. Boyce, R.C. DiPrima, "Elementary Differential Equations and Boundary Value Problems", John Wiley and Sons, 1977.
6. E.A. Guillemin, "A Historical Account of the Development Procedure for Pulse-Forming-Networks", RL Report No. 43, Oct. 16, 1944.
7. H.Y-F. Lam, "Analog and Digital Filters, Design and Realization", Prentice-Hall Inc., 1979.
8. N. Balabanian, T. Bickart, "Linear Network Theory", Matrix Publishers, Inc., 1981.
9. L.L. Reginato, D.B. Cummings, private communication at Lawrence Livermore Laboratory, 1988.
10. B.P. Lathi, "Signals, Systems, and Controls", Harper and Row, 1974.
11. T. J. Fessenden, D. Keefe, C. Kim, H. Meuth, A. Warwick, "The LBL Multiple Beam Experiments", 1987 Particle Accelerator Conference, Washington D.C., March 16-19, 1987.

12. M. Kristiansen, et. al., "Pulse Power Technology Lecture Notes", lecture notes of course taught at Lawrence Livermore National Laboratory, Feb.-May, 1988.